Tuning an output-only dual Kalman filter for displacement estimation from measured accelerations

A THESIS
SUBMITTED TO THE FACULTY OF THE
UNIVERSIY OF MINNESOTA
BY

Riley J. Brown

IN PARTIAL FULFILLMENT OF THE REQUIREMENTS
FOR THE DEGREE OF
MASTER OF SCIENCE

Lauren E. Linderman
Carol K. Shield

July 2019

Acknowledgement

I would like to acknowledge the support of the Minnesota Department of Transportation. I would also like to thank my advisors, Lauren Linderman and Carol Shield, for their guidance throughout this project.

Abstract

Direct measurement of the vertical displacement of bridge superstructures is typically not feasible; therefore, methods to estimate displacement from acceleration measurements exist. Joint input-state estimation techniques based on Kalman-type filters have been used for estimating displacements, but the task of tuning the filter is not straightforward. Therefore, this work explored a tuning procedure for the output-only implementation of the dual Kalman filter for displacement estimation via noisy acceleration measurements. The validity of the tuning procedure was demonstrated using simulated systems and experimental tests, and good dynamic displacement estimates were achieved in all cases. The approach indicated that model noise (e.g., due to poor system identification results) did not affect the tuning process as much as measurement noise. The output-only formulation of the problem caused the input estimates to lose physical meaning; however, the input estimator increased state estimation performance under various loading types as compared to a single Kalman filter.

Table of Contents

List of Tables

List of Figures

Chapter 1: Introduction

1.1 Problem Statement

Structural health monitoring is concerned with identifying problematic or damage-related behavior in a structure, with the ultimate goal of providing tools for aiding in structural maintenance and decision making (French et al. 2014). Studies have suggested the use of output-only vibration measurements for structural monitoring (Deraemaeker et al. 2008; Magalhães et al. 2012), but changing environmental conditions make damage detection difficult. A monitoring system on the I-35W Saint Anthony Falls Bridge, which crosses the Mississippi River in Minneapolis, MN, has been collecting vertical acceleration data since the construction of the bridge in 2008. Given the significant variation observed in the modal parameters of the bridge, changes in the dynamic signature of the structure alone were found to provide insufficient information to detect damage (Gaebler et al. 2017). Gaebler et al. (2017) proposed that vertical displacement, a simpler parameter with a more immediate physical meaning than natural frequency, was better suited to monitor the short-term behavior and long-term serviceability of the I-35W Saint Anthony Falls Bridge.

Vertical displacements are challenging to measure on structures like the I-35W Saint Anthony Falls Bridge without on-site surveying. Given that accelerometers are commonplace in monitoring efforts of civil structures, researchers have adopted state estimation methods to reconstruct the dynamic displacement response of vibrating systems through limited acceleration measurements (Eftekhar Azam et al. 2015a; Lourens et al. 2012a). These methods can theoretically provide optimal displacement estimates under certain conditions, but implementing the estimation methods on a civil system is not always straightforward. Therefore, the research conducted for this project was focused on a tuning procedure to implement a state estimation method to estimate the displacement response of a bridge structure from acceleration measurements.

1.2 Literature Review

Displacement profiles of structures are traditionally measured using linear variable differential transformers (LVDTs) in the laboratory, or using potentiometers and extensometers in

the field. LVDTs, potentiometers, and extensometers are contact-based displacement measurement methods that require a fixed reference point from which to measure relative displacements. When measuring vertical displacements in the laboratory, a common approach is to construct a scaffold under the desired measurement location and use the ground as fixed reference. However, the use of scaffolding for large-scale structures in the field is often impractical because it is costly, requires considerable time for assembly and disassembly, and, more importantly, requires unobstructed access to the desired measurement location from the ground (Gindy et al. 2008). This would exclude portions of bridges that span roadways and railways in which traffic cannot be stopped for the testing period and portions of bridges that traverse bodies of water or deep ravines, such as the I-35W Saint Anthony Falls Bridge, from vertical displacement measurement using contact-based sensors.

As an alternative to traditional measurement methods such as LVDTs, various non-contact measurement systems have been used to measure displacements. Similar to contact-based measurement systems, almost all non-contact measurement systems require a fixed reference point. Nassif et al. (2005) showed that non-contact laser Doppler vibrometer measurements compare very well with those recorded by LVDTs; however, laser vibrometers measure the differential displacement between an optical laser head and the measurement point, so the unit needs to be mounted on a support that is free of vibration. Typically the system is setup on the ground underneath the measurement point, which is impractical for structures spanning bodies of water. Vision-based displacement measurement methods have also been used as an alternative to contact-based displacement measurement techniques. Lee and Shinozuka (2006) proposed a real-time vision-based system that uses a digital video camera (with fixed location and telescopic device) to take a motion picture of a target installed at a measurement location. Displacement of the target is calculated using an image processing technique, which requires a target recognition algorithm, projection of the captured image, and calculation of the displacement using target geometry and number of pixels moved. Recent advances in computer vision techniques in conjunction with acquisition through unmanned aerial vehicles (UAVs) offer promising noncontact solutions to civil infrastructure condition assessment (e.g., crack detection) without requiring a fixed reference point, but the task of accurate dynamic displacement measurement for *in situ* civil infrastructure using UAVs requires further research (Spencer Jr. et al. 2019).

To avoid some of the difficulties associated with measuring displacement directly, researchers have proposed techniques to achieve displacement estimates indirectly through the

relationship between acceleration and displacement. Accelerometers are frequently used for vibration monitoring of civil structures, and, in theory, displacements can be determined by double integration of acceleration measurements. In practice, displacement estimates from integrated acceleration measurements tend to drift away from measured displacements due to incorrectly assumed initial conditions and small recording errors in the acceleration signal (Gindy et al. 2008). Numerous correction methods have been developed for minimizing the effect of errors that accumulate through successive integrations of the measured acceleration signal, and the correction methods can generally be implemented before or after integration of the measured accelerations. Gindy et al. (2008) proposed an analytical model based on a state-space approach that was used to obtain an approximate model of the noise-free acceleration signal which, when twice integrated, results in an estimated displacement signal. Unlike Gindy et al. (2008), which attempts to correct the displacement estimate by removing much of the noise in the measured acceleration signal, most other approaches correct the displacement estimate after integration of the measured noisy acceleration signal. If assuming zero initial conditions, a linear base line method can be used to remove a fitted line from the integrated acceleration signal prior to a second integration (Faulkner et al. 1996; Kropp 1977). If the initial conditions are not zero, however, the initial velocity estimation method (VEM) has been used to reduce the accumulation of error in displacement estimates from incorrect initial condition assumptions (Park et al. 2005). The VEM is an iterative procedure that estimates initial bridge velocity while assuming a zero initial displacement and is carried out until zero average velocity is achieved, thereby ensuring no permanent drift at the end of the signal. With all integration techniques, the accumulation of error in the displacement estimate tends to increase with longer acceleration signal segments.

As an alternative to successively integrating acceleration measurements, some researchers have approached the problem from a control theory perspective through state estimation. Any set of differential equations can be transformed into a coupled set of first order equations, called the state-space form, as a general way of representing the dynamics of a linear system. When modeling physical processes, model/process noise and measurement noise are typically included in the system equations to improve estimation of system response in the presence of uncertainties. In the context of estimating displacements from acceleration, state estimation refers to the process of identifying quantities that completely describe the system state (e.g. displacements, velocities), based on a system model (e.g. relationship between displacement, velocity, and acceleration), from the system output (e.g. acceleration measurements). Estimating the true state of a system is an extensively studied problem, and various state estimators have

been proposed for applications to civil engineering problems. A technique that has seen success for displacement estimation from noisy acceleration measurements is the Kalman filter (Kalman 1960), as the Kalman filter is the optimal time-varying solution to the linear estimation problem (Franklin et al. 1998).

Joint input-state estimation refers to the process of estimating both the unknown states and unknown inputs of a system. For large-scale civil structures, it is generally not possible to measure the input to the system or accurately predict the driving forces. Prior to joint input-state estimation methods being used for civil applications, a common approach was to model the input force as a zero-mean white Gaussian process and make use of Bayesian techniques for state estimation (Gillijns and De Moor 2007; Lourens et al. 2012a). This approach can provide reasonable state estimates in some circumstances, but it may provide unacceptable state estimates when the loading assumption is violated. So as to identify the unknown forces in a stochastic manner, Lourens et al. (2012b) included the unknown forces in the state vector and estimated the input to the system in conjunction with the states using an augmented Kalman filter. The augmented Kalman filter method tends to have numerical instabilities due to unobservability issues of the augmented system matrix, and Maes et al. (2015) later derived the conditions for the invertibility of linear system models that apply to any instantaneous input estimation or joint input-state estimation algorithm. Eftekhar Azam et al. (2015a; b) combined two separate Kalman filters (aptly named the dual Kalman filter) for joint input-state estimation; and demonstrated that by fine-tuning the regulatory parameters of the filter, the successive structure of the dual Kalman filter resolves the numerical issues attributed to unobservability and rank deficiency of the augmented formulation of the problem.

Tuning the parameters of the estimation system refers to proper selection of the noise covariance matrices that represent the stochastic part of the system model. The specified noise characteristics of a system have significant effects on the quality of the state estimate, and traditional Kalman filters require exact knowledge of the process noise covariance matrix and measurement noise covariance matrix for optimal estimation. For the dual Kalman filter, an additional input noise covariance matrix is present to model the uncertainties associated with the input system model. As such, specification of three covariance matrices (i.e., process noise covariance matrix, input noise covariance matrix, and measurement noise covariance matrix) is required. Typically, the stochastic part of the system model is difficult to quantify, and the covariance matrices are only known approximately, if at all.

One approach to quantify the stochastic part of the system is by estimating the noise covariance matrices in the state and measurement equations of the model. Noise covariance matrix estimation methods found in the literature are based on using the measured data to find the noise covariance matrices. Duník et al. (2017) provides an in-depth survey of many noise covariance matrix estimation procedures, which are usually divided into four groups: correlation methods (Mehra 1970), maximum-likelihood methods (Shumway and Stoffer 2000), covariance matching methods (Myers and Tapley 1976), and Bayesian methods (Lainiotis 1971). The area of noise covariance matrix estimation is well established, but many filter designers rely on the simpler practice of utilizing user-defined covariance matrices.

Utilization of user-defined noise covariance matrices intrinsically results in suboptimal filter designs, as the optimal filter design would coincide with one using the true noise covariance matrices describing the physical system being modeled, but the practice is simple and can provide filter designs that perform acceptably. Typically, the form of the noise covariance matrices are chosen by the user, and a scalar coefficient is treated as a tunable parameter in the estimator design. Once the form of the covariance matrices are chosen by the filter designer, L-curve-type approaches can be used to choose good (i.e., nearly optimal) parameters for the noise covariance matrices. L-curves are a convenient way to display information about the estimator design as a function of the tuning parameter, and they provide a visual from which an intuitive selection for the regularization parameter can be chosen. Traditionally, L-curves are a plot of the norm of the estimated solution versus the estimation residual norm (i.e., the norm of the difference between the estimated and the measured quantities) for different values of the regularization parameter. Hansen (1992) provides an in-depth exploration of L-curves.

The values of the regularization parameter obtained through the L-curve are associated with the (nearly) optimal estimates for the observed quantity (i.e., acceleration measurements). However, this does not necessarily coincide with the most accurate estimate of the unobserved quantities, namely the displacement, velocity, and input estimates (Eftekhar Azam et al. 2015b). In the case of the augmented Kalman filter, Lourens et al. (2012b) treated the covariance matrix describing the noise of the force increments as the regularization parameter, and noticed that the curve representing the square of the norm of the identified force as a function of the error norm (i.e., the norm of the difference between the measured accelerations and accelerations computed using the state and input estimates) does not exhibit its classical L-shape. This behavior was explained by the fact that the error norm for the augmented Kalman filter depends on the force as

well as on the state estimates. A similar observation of a not so classic L-curve was made by Eftekhar Azam et al. (2015b) when using the dual Kalman filter. In instances using the augmented Kalman filter and the dual Kalman filter, choosing the regularization parameter by means of a traditional L-curve is not a straightforward task (Eftekhar Azam et al. 2015b).

To aid in tuning the dual Kalman filter, Eftekhar Azam et al. (2015b) introduced a complimentary metric that relies on the plot of the filter regularization parameter against the error norm. The covariance matrix describing the fictitious input noise was treated as the regularization parameter and the error norm was the norm of the known error in the acceleration estimate, which was the same as that used in Lourens et al. (2012b). Since its introduction, this L-curve-type tuning approach has been a common method for finding an appropriate level of regularization for the dual Kalman filter.

In using this tuning method for the dual Kalman filter, most authors assume prior knowledge of the process noise covariance matrix and measurement noise covariance matrix (Eftekhar Azam et al. 2015a; b; Petersen et al. 2018; Tatsis and Lourens 2016). Doing so allows the input noise covariance matrix to be treated as the single tuning parameter of the system. In most scenarios, the chosen process noise covariance is a "best practice" solution without a true basis from optimal theory (Petersen et al. 2018).

However, knowledge of the process noise covariance matrix *a priori* may not be possible in all scenarios, especially when the system model is constructed using output-only system identification techniques. Generating a system model using modal information from output-only system identification methods has considerable advantages over, for example, a complicated finite element model. Finite element models require significant time and effort to ensure that they accurately reflect the physical structure. When estimating displacements from accelerations, the accelerometers necessary for system identification would already be in place; and using identification results near the time of desired estimation would ensure an updated system model (Gaebler 2017). Even when minimizing model uncertainty using the most up-to-date system identification, the process noise is still difficult to quantify. In addition to instances when the process noise covariance matrix is not known, the filter designer may wish to understand the implications of the process noise covariance selection on the filter estimates. In such scenarios, the process noise covariance matrix should be treated a second tuning parameter of the system.

1.3 Research Approach and Outline

This work highlights a tuning process for use with an output-only formulation of the dual Kalman filter for joint input-state estimation. When constructing a system model from a typical output-only system identification technique, the structural mass information is unknown. Therefore, approximations are typically taken in the formulation of the system equations that cause the input estimates to lose physical meaning. The tuning process for selecting the noise covariance matrices used by previous researchers is modified in a way that the process noise covariance and input noise covariance are treated as user-defined tuning parameters. The noise covariance matrices are assumed to be diagonal, and the magnitude of the diagonal elements are tuned to provide acceptable estimation performance. Various systems are considered, both numerical and experimental, and the effects of system damping, model and measurement noise, and model truncation on the tuning process are highlighted. The relationship between the tuning parameters associated with the optimal estimate of the observed acceleration and the tuning parameters associated with the optimal estimate of the unobserved displacement is also documented.

Chapter 2 contains the output-only formulation of the linear state-space equations to be used with the dual Kalman filter. An explanation on how the dual Kalman filter is used and implemented for joint input-state estimation is included. Chapter 3 focuses on tuning the dual Kalman filter for a simulated spring-mass-damper system. In Chapter 4 the output-only formulation of the problem is validated via a simulated blind case study. Chapter 5 discusses the advantage of using the dual Kalman filter over a traditional, single Kalman filter when the input estimates are not of concern. Conclusions on the tuning procedure are given in Chapter 6.

Chapter 2: System model equations and the dual Kalman filter

In this chapter, a stochastic state-space representation of a discrete system is formulated for implementation of the dual Kalman filter using an output-only system model. First, the equations of motion are used to generate the model and measurement equations of a discretized system in state-space form. The equations are modified to account for an output-only implementation with unknown structural mass. Then, the dual Kalman filter algorithm is introduced to jointly estimate both inputs (i.e., external forces) and states (i.e., displacement and velocity) from measured accelerations.

2.1 State-space system equations

Consider the equations of motion for a discretized system

$$\mathbf{M}\ddot{\mathbf{u}}(t) + \mathbf{C}\dot{\mathbf{u}}(t) + \mathbf{K}\mathbf{u}(t) = \mathbf{f}(t) = \mathbf{S}_{\mathrm{p}}\mathbf{p}(t) \tag{1}$$

where $\mathbf{u}(t) \in \mathbb{R}^n$ is a displacement vector, $\mathbf{M}$, $\mathbf{C}$, and $\mathbf{K} \in \mathbb{R}^{n \times n}$ represent the mass, damping, and stiffness matrix, respectively, for an n degree of freedom system. A single dot and double dot over a vector denote first and second time derivatives, respectively. The excitation force vector $\mathbf{f}(t) \in \mathbb{R}^n$ can be represented as a superposition of p input time histories $\mathbf{p}(t) \in \mathbb{R}^p$ modified by an influence matrix $\mathbf{S}_{\mathrm{p}} \in \mathbb{R}^{n \times p}$.

When using output-only system identification methods, the problem is conveniently formulated in modal coordinates. The undamped eigenvalue problem corresponding to Eq. (1) is written:

$$\mathbf{K}\boldsymbol{\Phi} = \mathbf{M}\boldsymbol{\Phi}\boldsymbol{\Omega}^2 \tag{2}$$

where the solution gives the mode shapes, $\boldsymbol{\Phi} \in \mathbb{R}^{n \times n}$, and natural frequencies, $\boldsymbol{\Omega} \in \mathbb{R}^{n \times n}$, of the system. Introducing the coordinate transformation:

$$\mathbf{u}(t) = \boldsymbol{\Phi}\mathbf{z}(t) \tag{3}$$

where $\mathbf{z}(t) \in \mathbb{R}^n$ and premultiplying Eq. (1) by $\boldsymbol{\Phi}^T$, the equation of motion is rewritten in modal coordinates as:

$$\boldsymbol{\Phi}^{\mathrm{T}}\mathbf{M}\boldsymbol{\Phi}\ddot{\mathbf{z}}(t) + \boldsymbol{\Phi}^{\mathrm{T}}\mathbf{C}\boldsymbol{\Phi}\dot{\mathbf{z}}(t) + \boldsymbol{\Phi}^{\mathrm{T}}\mathbf{K}\boldsymbol{\Phi}\mathbf{z}(t) = \boldsymbol{\Phi}^{\mathrm{T}}\mathbf{S}_{\mathrm{p}}\mathbf{p}(t) \tag{4}$$

The dynamic response of civil structures is typically dominated by a limited number of vibration modes, and therefore a limited number of modes are identifiable by output-only methods. A truncated modal space could be substituted in Eq. (3) such that the modal matrix $\boldsymbol{\Phi}_{\mathrm{m}} \in \mathbb{R}^{n \times m}$ consists of the first m mode shapes as columns, where $m < n$, and $\mathbf{z}_{\mathrm{m}}(t) \in \mathbb{R}^{m}$. The subscript m denotes matrices associated with the truncated modal space with m modes. Assuming proportional damping and that the orthogonality property of the mode shapes holds ($\boldsymbol{\Phi}_{\mathrm{m}}^{\mathrm{T}}\mathbf{M}\boldsymbol{\Phi}_{\mathrm{m}}$ is diagonal), Eq. (4) can be premultiplied by $(\boldsymbol{\Phi}_{\mathrm{m}}^{\mathrm{T}}\mathbf{M}\boldsymbol{\Phi}_{\mathrm{m}})^{-1}$ to arrive at a set of m decoupled equations:

$$\ddot{\mathbf{z}}_{\mathrm{m}}(t) + \boldsymbol{\Gamma}_{\mathrm{m}}\dot{\mathbf{z}}_{\mathrm{m}}(t) + \boldsymbol{\Omega}_{\mathrm{m}}^{2}\mathbf{z}_{\mathrm{m}}(t) = (\boldsymbol{\Phi}_{\mathrm{m}}^{\mathrm{T}}\mathbf{M}\boldsymbol{\Phi}_{\mathrm{m}})^{-1}\boldsymbol{\Phi}_{\mathrm{m}}^{\mathrm{T}}\mathbf{S}_{\mathrm{p}}\mathbf{p}(t) \tag{5}$$

where $\boldsymbol{\Omega}_{\mathrm{m}} \in \mathbb{R}^{m \times m}$ is a diagonal matrix which contains the natural frequencies ω_i $(i = 1, \dots, m)$ in radians per second and $\boldsymbol{\Gamma}_{\mathrm{m}} \in \mathbb{R}^{m \times m}$ contains entries of the form $2\zeta_i\omega_i$ on the diagonal, where ζ_i denotes the modal damping ratio.

By introducing the state vector $\mathbf{x}(t) \in \mathbb{R}^{s}$, where $s = 2m$ stands for the number of states, Eq. (5) can be represented as a continuous-time state equation:

$$\dot{\mathbf{x}}(t) = \mathbf{A}_{\mathrm{c}}\mathbf{x}(t) + \mathbf{B}_{\mathrm{c}}\mathbf{p}(t), \qquad \mathbf{x}(t) = \begin{bmatrix}\mathbf{z}_{\mathrm{m}}(t)\\ \dot{\mathbf{z}}_{\mathrm{m}}(t)\end{bmatrix} \tag{6}$$

with system matrices:

$$\mathbf{A}_{\mathrm{c}} = \begin{bmatrix}\mathbf{0} & \mathbf{I}\\ -\boldsymbol{\Omega}_{\mathrm{m}}^{2} & -\boldsymbol{\Gamma}_{\mathrm{m}}\end{bmatrix}, \qquad \mathbf{B}_{\mathrm{c}} = \begin{bmatrix}\mathbf{0}\\ (\boldsymbol{\Phi}_{\mathrm{m}}^{\mathrm{T}}\mathbf{M}\boldsymbol{\Phi}_{\mathrm{m}})^{-1}\boldsymbol{\Phi}_{\mathrm{m}}^{\mathrm{T}}\mathbf{S}_{\mathrm{p}}\end{bmatrix}$$

The problem is formulated assuming that only acceleration measurements are available, and that the measurement locations define the n degrees of freedom of the discrete system. The acceleration measurement vector $\mathbf{y}(t) \in \mathbb{R}^{n}$ is expressed in terms of the state and input using the equation of motion to arrive at a state-space measurement equation:

$$\mathbf{y}(t) = \mathbf{C}_{\mathrm{c}}\mathbf{x}(t) + \mathbf{D}_{\mathrm{c}}\mathbf{p}(t) \tag{7}$$

where the measurement matrix $\mathbf{C}_{\mathrm{c}}$ and direct transmission matrix $\mathbf{D}_{\mathrm{c}}$ are:

$$\mathbf{C}_{\mathrm{c}} = [-\boldsymbol{\Phi}_{\mathrm{m}}\boldsymbol{\Omega}_{\mathrm{m}}^{2} \quad -\boldsymbol{\Phi}_{\mathrm{m}}\boldsymbol{\Gamma}_{\mathrm{m}}], \qquad \mathbf{D}_{\mathrm{c}} = \left[\boldsymbol{\Phi}_{\mathrm{m}}(\boldsymbol{\Phi}_{\mathrm{m}}^{\mathrm{T}}\mathbf{M}\boldsymbol{\Phi}_{\mathrm{m}})^{-1}\boldsymbol{\Phi}_{\mathrm{m}}^{\mathrm{T}}\mathbf{S}_{\mathrm{p}}\right]$$

2.2 Output-only implementation

When using output-only models, $\mathbf{M}$ is generally unknown. In such a situation, mass normalization of mode shapes is impossible and an approximation on the system matrices $\mathbf{B_c}$ and $\mathbf{D_c}$ is required. The accuracy of the approximation, with respect to the real system, dictates whether or not the input estimates hold physical meaning. In the case that the approximation accurately reflects the physical system, $\mathbf{p}(t)$ represents force time histories and the loading on the structure. When the positions of the applied forces are unknown, the inputs $\mathbf{p}(t)$ become a set of equivalent forces acting at the location of the acceleration measurements which would produce the same measured response (Lourens et al. 2012a). A more likely scenario is an inaccurate approximation of the system matrices, in which case the input estimates lose physical meaning. In order to satisfy Eq. (7) for a given acceleration measurement and state, $\mathbf{p}(t)$ must absorb the inaccuracies associated with the approximation made on $\mathbf{D_c}$.

In this study, $(\boldsymbol{\Phi}_\mathrm{m}^\mathrm{T}\mathbf{M}\boldsymbol{\Phi}_\mathrm{m})^{-1}$ was assumed to equal the identity matrix of appropriate dimension and mode shapes were normalized such that the maximum relative displacement was unity. The assumed continuous-time state-space equations are rewritten as:

$$\begin{aligned} \dot{\mathbf{x}} &= \mathbf{A}_\mathrm{c}\mathbf{x}(t) + \mathbf{B}_\mathrm{p}\mathbf{p}(t) \\ \mathbf{y}(t) &= \mathbf{C}_\mathrm{c}\mathbf{x}(t) + \mathbf{D}_\mathrm{p}\mathbf{p}(t) \end{aligned} \tag{8}$$

$$\mathbf{A}_\mathrm{c} = \begin{bmatrix} \mathbf{0} & \mathbf{I} \\ -\boldsymbol{\Omega}_\mathrm{m}^2 & -\boldsymbol{\Gamma}_\mathrm{m} \end{bmatrix}, \qquad \mathbf{B}_\mathrm{p} = \begin{bmatrix} \mathbf{0} \\ \boldsymbol{\Phi}_\mathrm{m}^\mathrm{T}\mathbf{S}_\mathrm{p} \end{bmatrix},$$
$$\mathbf{C}_\mathrm{c} = \begin{bmatrix} -\boldsymbol{\Phi}_\mathrm{m}\boldsymbol{\Omega}_\mathrm{m}^2 & -\boldsymbol{\Phi}_\mathrm{m}\boldsymbol{\Gamma}_\mathrm{m} \end{bmatrix}, \qquad \mathbf{D}_\mathrm{p} = \begin{bmatrix} \boldsymbol{\Phi}_\mathrm{m}\boldsymbol{\Phi}_\mathrm{m}^\mathrm{T}\mathbf{S}_\mathrm{p} \end{bmatrix}$$

2.3 Discrete-time stochastic state-space equations

For use with stochastic estimation approaches using measured data, the continuous-time state-space equations are represented in discrete time with appropriate noise vectors. Eq. (8) can be implemented in discrete time with a sampling rate $1/\Delta t$ such that discrete time instants are defined by $t_k = k\,\Delta t$, for $k = 1, 2, \ldots, N_t$. Under the assumption of a zero-order hold on the input, the discrete-time state-space equations are:

$$\mathbf{x}_{k+1} = \mathbf{A}_d \mathbf{x}_k + \mathbf{B}_d \mathbf{p}_k$$
$$\mathbf{y}_k = \mathbf{C}_d \mathbf{x}_k + \mathbf{D}_d \mathbf{p}_k \tag{9}$$

where $\mathbf{A}_\mathrm{d} = \exp(\mathbf{A}_\mathrm{c} \Delta t)$, $\mathbf{B}_\mathrm{d} = [\mathbf{A}_\mathrm{c} - \mathbf{I}]\mathbf{A}_\mathrm{c}^{-1}\mathbf{B}_\mathrm{p}$, $\mathbf{C}_\mathrm{d} = \mathbf{C}_\mathrm{c}$, and $\mathbf{D}_\mathrm{d} = \mathbf{D}_\mathrm{p}$. Eq. (9) is represented stochastically with the addition of process noise $\mathbf{w}_k^\mathrm{x} \in \mathbb{R}^s$ and measurement noise $\mathbf{v}_\mathrm{k} \in \mathbb{R}^n$ vectors:

$$\mathbf{x}_{k+1} = \mathbf{A}_\mathrm{d} \mathbf{x}_k + \mathbf{B}_\mathrm{d} \mathbf{p}_k + \mathbf{w}_k^\mathrm{x}$$
$$\mathbf{y}_k = \mathbf{C}_\mathrm{d} \mathbf{x}_k + \mathbf{D}_\mathrm{d} \mathbf{p}_k + \mathbf{v}_k \tag{10}$$

The process noise and measurement noise vectors were assumed to be uncorrelated, zero-mean, white noise signals with covariance matrices $\mathbf{Q}^\mathrm{x} \in \mathbb{R}^{s \times s}$ and $\mathbf{R} \in \mathbb{R}^{n \times n}$, respectively.

2.4 Dual Kalman filter for input and state estimation

The dual Kalman filter (DKF) was used to estimate the unknown input $\mathbf{p}_k$ and unknown state $\mathbf{x}_k$ of the Eq. (10) system using the noisy acceleration measurements $\mathbf{y}_k$. The DKF scheme is divided into two stages: a Kalman filter to estimate the input and a Kalman filter to estimate the system state. Input estimation is accomplished by introducing a fictitious process equation that serves to propagate the input forward in time:

$$\mathbf{p}_{k+1} = \mathbf{p}_k + \mathbf{w}_k^\mathrm{p} \tag{11}$$

where $\mathbf{w}_k^\mathrm{p} \in \mathbb{R}^p$ is an assumed zero-mean, white noise process with covariance matrix $\mathbf{Q}^\mathrm{p} \in \mathbb{R}^{p \times p}$.

The general scheme for the dual Kalman filter, as described by Eftekhar Azam et al. (2015a), is as follows:

- Initialization at time t_0

$$\hat{\mathbf{p}}_0 = \mathbb{E}[\mathbf{p}_0]$$
$$\mathbf{P}_0^\mathrm{p} = \mathbb{E}[(\mathbf{p}_0 - \hat{\mathbf{p}}_0)(\mathbf{p}_0 - \hat{\mathbf{p}}_0)^\mathrm{T}]$$
$$\hat{\mathbf{x}}_0 = \mathbb{E}[\mathbf{x}_0]$$
$$\mathbf{P}_0^\mathrm{x} = \mathbb{E}[(\mathbf{x}_0 - \hat{\mathbf{x}}_0)(\mathbf{x}_0 - \hat{\mathbf{x}}_0)^\mathrm{T}]$$

- At time t_k, for $k = 1, \ldots, N_t$:
  - Prediction stage for the input:
    1. Evolution of the input and prediction of covariance input:

$$\mathbf{p}_k^- = \mathbf{p}_{k+1}$$
$$\mathbf{P}_k^{\mathrm{p}-} = \mathbf{P}_{k-1}^{\mathrm{p}} + \mathbf{Q}^{\mathrm{p}}$$

  - Update stage for the input:
    2. Calculation of Kalman gain for input:

$$\mathbf{G}_k^{\mathrm{p}} = \mathbf{P}_k^{\mathrm{p}-}\mathbf{D}_{\mathrm{d}}^{\mathrm{T}}(\mathbf{D}_{\mathrm{d}}\mathbf{P}_k^{\mathrm{p}-}\mathbf{D}_{\mathrm{d}}^{\mathrm{T}} + \mathbf{R})^{-1}$$

    3. Improve predictions of input using latest observation:

$$\hat{\mathbf{p}}_k = \mathbf{p}_k^- + \mathbf{G}_k^{\mathrm{p}}(\mathbf{y}_k - \mathbf{C}_{\mathrm{d}}\hat{\mathbf{x}}_{k-1} - \mathbf{D}_{\mathrm{d}}\mathbf{p}_k^-)$$
$$\mathbf{P}_k^{\mathrm{p}} = \mathbf{P}_k^{\mathrm{p}-} - \mathbf{G}_k^{\mathrm{p}}\mathbf{D}_{\mathrm{d}}\mathbf{P}_k^{\mathrm{p}-}$$

  - Prediction stage for the state:
    4. Evolution of state and prediction of covariance of state:

$$\mathbf{x}_k^- = \mathbf{A}_{\mathrm{d}}\hat{\mathbf{x}}_{k-1} + \mathbf{B}_{\mathrm{d}}\hat{\mathbf{p}}_k$$
$$\mathbf{P}_k^{\mathrm{x}-} = \mathbf{A}_{\mathrm{d}}\mathbf{P}_{k-1}^{\mathrm{x}}\mathbf{A}_{\mathrm{d}}^{\mathrm{T}}\mathbf{A}^{\mathrm{T}} + \mathbf{Q}^{\mathrm{x}}$$

  - Update stage for the state:
    5. Calculation of Kalman gain for state:

$$\mathbf{G}_k^{\mathrm{x}} = \mathbf{P}_k^{\mathrm{x}-}\mathbf{D}_{\mathrm{d}}^{\mathrm{T}}(\mathbf{D}_{\mathbf{d}}\mathbf{P}_k^{\mathrm{x}-}\mathbf{D}_{\mathrm{d}}^{\mathrm{T}} + \mathbf{R})^{-1}$$

    6. Improve predictions of state using latest observation:

$$\hat{\mathbf{x}}_k = \mathbf{x}_k^- + \mathbf{G}_k^{\mathrm{x}}(\mathbf{y}_k - \mathbf{C}_{\mathrm{d}}\mathbf{x}_k^- - \mathbf{D}_{\mathrm{d}}\hat{\mathbf{p}}_k)$$
$$\mathbf{P}_k^{\mathrm{x}} = \mathbf{P}_k^{\mathrm{x}-} - \mathbf{G}_k^{\mathrm{x}}\mathbf{C}_{\mathrm{d}}\mathbf{P}_k^{\mathrm{x}-}$$

The dual Kalman filter procedure required initial information on the expected value and covariance of the state ($\hat{\mathbf{x}}_0$ and $\mathbf{P}_0^{\mathrm{x}}$, respectively) and input ($\hat{\mathbf{p}}_0$ and $\mathbf{P}_0^{\mathrm{p}}$, respectively). For all implementations of the dual Kalman filter in this manuscript, the initial expected value of all state and input variables was zero. The initial covariance matrices of the state and input were assumed to be fully populated with ones. This assumption did not accurately reflect the joint variability of the elements of the state and input vectors, however impact of the assumption on the final state estimates was minor due to the steady state implementation of the filter described in greater detail in Chapter 3.

Chapter 3: Tuning the dual Kalman filter

The following sections contain examples of a simulated system that were explored to highlight the process of tuning the dual Kalman filter for displacement estimation from acceleration measurements. The tuning procedure is introduced first in Section 3.1. Then the system on which the tuning procedure is utilized is presented in Section 3.2. Section 3.3 presents an investigation of added system noise and its effects on tuning.

3.1 Tuning procedure for $\mathbf{Q}^{\mathrm{x}}$ and $\mathbf{Q}^{\mathrm{p}}$

Tuning refers to proper selection of the noise covariance matrices $\mathbf{Q}^{\mathrm{x}}$, $\mathbf{Q}^{\mathrm{p}}$, and $\mathbf{R}$ to achieve accurate estimates of the unobserved state and input. Because measurements are necessary to operate the dual Kalman filter, it is usually possible to quantify the measurement noise covariance $\mathbf{R}$ prior to implementing the filter. The measurement noise is based on the sensitivity of the sensors used to measure the accelerations, and the variance of each sensor can be quantified by manufacture specifications and tests to determine the sensor noise floor. In tuning the other noise covariance matrices, the input noise covariance matrix and process noise covariance were assumed to take the form $\mathbf{Q}^{\mathrm{p}} = Q^{p} \times \mathbf{I}$ and $\mathbf{Q}^{\mathrm{x}} = Q^{x} \times \mathbf{I}$, respectively, where Q^{p} and Q^{x} were scalar quantities. Such an assumption is typical when no information on the cross-correlation of the noise elements is available (Franklin et al. 1998). The magnitudes of Q^{p} and Q^{x} were the variances of the noise components, and Q^{p} and Q^{x} were treated as the tuning parameters of the system.

Because the accuracy of the estimates, and therefore the accuracy of the tuning procedure, could only be judged if the true state and input were known, estimated quantities were compared to the true simulation response and excitation to gain insight on the effects of tuning. To simplify this comparison, a steady state form of the DKF algorithm presented in Chapter 2 was used for estimation. Due to the formulation of the input estimator, numerical instabilities arose when trying to solve for the steady state gains prior to implementing the filter. Therefore, the time-varying DKF was run until steady state was reached, and then a time-invariant DKF was applied to the entire time history using the steady state gains. The time-invariant filter allowed for comparison of the entire response and estimate time histories without having to account for the stabilization time of the filter. Additionally, the system was assumed to be time-invariant over the

estimation time considered; updates to the output-only model to reflect system changes was assumed to occur prior to implementing the filter.

In most practical settings, the noise covariance matrices needed to implement the DKF are unknown. Several works in the literature provide rule-of-thumb methods to appropriately tune the filter, however most authors assume prior knowledge of the process noise Q^x. With that assumption, the covariance of the input noise Q^p acts as a single tuning parameter for the DKF, and L-curve-type approaches are often taken to select the input covariance Q^p (Eftekhar Azam et al. 2015a; Lourens et al. 2012b; Petersen et al. 2018; Tatsis and Lourens 2016). Such an assumption is difficult to make when constructing a model using output-only system identification results, where the amount of uncertainty in the model may be unknown. For the output-only formulation of the problem in this work, no knowledge of the process noise covariance parameter Q^x was assumed *a priori*, and Q^x was treated as a second tuning parameter of the system.

To tune the filter, the dual Kalman filter algorithm was implemented for various combinations of Q^x and Q^p and the response of the structure was estimated from the acceleration measurements. After the entire time history was estimated, two separate metrics were used to judge the performance of the DKF.

One metric looked at the norm of the estimation error for the measured quantities $\sum\|\mathbf{y}_k - (\mathbf{C}_\mathrm{d}\mathbf{x}_k^- + \mathbf{D}_\mathrm{d}\hat{\mathbf{p}}_k)\|_2^2 / N_t$ over the tunable range of Q^x and Q^p. This was analogous to the L-curve type approach used in Eftekhar Azam et al. (2015a), only expanded in the Q^p dimension to allow proper selection of the process noise covariance. All measured quantities were assumed to be accelerations, therefore this metric quantified the error of the acceleration estimates (from estimated states and inputs) as compared to the measured accelerations. The tunable range for Q^x and Q^p is difficult to define prior to computing the estimates, however values larger than and smaller than the magnitude of the measurement noise covariance should be considered. The plot of this acceleration error-metric as a function of the tuning parameters Q^x and Q^p is the main tool used to tune the dual Kalman filter.

A second metric was used to judge the performance of the estimator and measured the accuracy of the unobserved displacement state estimates with respect to the true state response. In practice, this comparison is impossible as displacement measurements were assumed unavailable. For simulations, however, the exact, noise-free displacement response was available, and the

comparison was possible. The average root mean squared error over all degrees of freedom $\sum_{n_{DOF}}\left(\sqrt{\sum_k\left(\mathrm{x_{k,act}}-\mathrm{x_{k,est}}\right)^2/N_t}\right)/n_{dof}$ was the metric adopted to compare the simulated and estimated displacements.

These two metrics, one to evaluate the accuracy of the acceleration measurements and one to evaluate the accuracy of the displacement estimates, are analyzed jointly to provide insight on how to tune for proper estimation of the unobserved displacement state from only knowledge of the acceleration error.

3.2 Simulated system

To assess the method of tuning the dual Kalman filter, a simulated 8 degree of freedom (DOF) system was considered. The system was a series of masses connected to each other with identical spring/damper couplings, with the first and last masses connected with the same coupling to fixed supports, as shown in Figure 1. Each node had a mass of 1 kg and the stiffness between each mass was 200 N/m. The modal damping ratio of each mode was varied depending on the case under consideration but was set at 2% for the initial discussion. The properties of this system were motivated by the I-35W Saint Anthony Falls Bridge in Minneapolis, MN; the mass and stiffness of the simulated system were chosen to produce natural frequencies that closely matched those identified on the I-35W Saint Anthony Falls Bridge (Gaebler et al. 2017).

The implementation of the dual Kalman filter was based on the simulated measurements generated by subjecting the system to a spatially correlated white noise excitation at each node. For each node, the same white noise signal was randomly shifted in time, with an average lag of 0.1 seconds. This excitation was used to approximate the correlated input at different nodes expected in a civil structure. The full system response was simulated in discrete time with a sampling rate of 100 Hz. Acceleration time histories from each node were used as measurements in the DKF, with varying amounts of Gaussian white noise added to simulate measurement noise.

3.3 Investigation of noise and its effects on tuning

In this section, the dual Kalman filter is used to estimate the response of the system defined in Section 3.2 subjected to a spatially correlated white noise excitation at each node,

using the tuning procedure described in Section 3.1. First, the response of the system was estimated using the true system parameters (with no added model or measurement noise) to introduce the tuning curves and to provide a baseline case from which to make comparisons. Then, the effects of system damping, model and measurement noise, and model truncation on the tuning process were investigated.

3.3.1 Tuning when no noise is present

The dual Kalman filter algorithm was implemented using the true modal parameters within the system model and using acceleration measurements with no added noise (i.e. clean model, clean measurements). The filter algorithm was executed assuming a measurement noise covariance of $\mathbf{R} = R \times \mathbf{I}$, where $R = 10^{-7}$. The magnitude of the measurement noise was chosen to match that seen in the data collected from accelerometers on the I-35W Saint Anthony Falls Bridge. Displacement estimates were generated over the range $Q^x = [10^{-20}, 10^{-5}]$ and $Q^p = [10^{-20}, 10^{0}]$. A selection of the generated displacement estimates at node 4 is shown in Figure 2, which highlights the significant effect of tuning on the displacement estimates. Figure 3 shows the power spectrum of the displacement estimates of Figure 2. Some displacement estimates had considerably larger high frequency content than others, which depended on the assumed level of process noise and input noise. Selection of the best (i.e., nearly optimal) tuning parameters based solely on the displacement estimates shown in Figure 3.

To aid in determining the best tuning parameters, the two error metrics were plotted as surfaces over the range of Q^x and Q^p, as shown in Figure 4a and Figure 4b. The two axes of the horizontal plane represent the tuning parameters of the displacement and input force estimation systems. Increasing values of the input noise covariance Q^p and process noise covariance Q^x, as compared to the fixed measurement noise covariance R, coincided with a relative increase in trust in the acceleration measurements. The lowest point on the displacement error surface (Figure 4b) located the tuning parameters with which the best displacement estimates were generated. The difficulty of using this tuning method lied in finding the optimal combination of Q^x and Q^p based solely on the acceleration error surface and estimated displacements (i.e. without knowledge of the exact displacements).

In keeping with an L-curve approach based on the acceleration error metric, an input noise covariance of $Q^p = 10^{-7}$ was chosen intuitively from Figure 4a. However, proper

selection of Q^x was difficult as it does not appear to affect the acceleration error for certain values of Q^p. From the displacement error surface (Figure 4b), any process noise covariance less than $Q^x = 10^{-15}$ with $Q^p = 10^{-7}$ gave the best displacement estimate. For this case, the tuning parameters producing the best displacement estimates suggested that when relatively less trust was placed in the input estimator, more accurate displacement estimates were achieved.

When implementing this tuning procedure in the field, the displacement error surface is unknown. Therefore, a modified representation of the acceleration error surface was required to determine the appropriate tuning parameters. Figure 4b shows several flat portions on the displacement error surface, which are highlighted with bold rectangular outlines. The combination of tuning parameters contained within each of the flat regions yielded essentially the same displacement error, and thus provided displacement estimates that were nearly identical. The flat regions from the displacement error surface were superimposed onto the acceleration error surface in Figure 4a. These four flat regions could be roughly identified from the acceleration errors only; the large flat region on the lower plane was divided by projecting the location of the valley on the upper surface. The identification of these flat regions from acceleration error, in turn, were used to locate a region in which tuning makes a difference on displacement estimates. Figure 5 shows the region of tuning parameters that generate all the possible displacement estimates (hexagon hatch), which was identified by the connecting lines of the four flat regions (diagonal hatch).

Given that the displacement measurements were not available for field implementations, the range of possible displacement estimates (as seen in Figure 2) generated from the identified region of tuning parameters (hexagon hatch in Figure 5) was inspected to select the tuning parameters that provided an estimate that was acceptable. Of course, this required judgement on the true response of the structure, from which there should be some form of engineering backing. Examples of judgement traits could include overall magnitude of the time history peaks or frequency content of the estimates, compared to what would be expected for the structure under consideration. For example, displacement estimates that contain the largest peak magnitudes in the time history while remaining a relatively smooth signal may be a good choice. In Figure 2, these properties were reflected by the displacement estimate generated assuming $Q^x = 10^{-18}$ and $Q^p = 10^{-6}$, which happened to provide displacement estimates that matched the true response well. The tuning parameters $Q^x = 10^{-17}$ and $Q^p = 10^{-6}$ provided the state estimates with the lowest displacement error.

For the case with a perfect system and perfect measurements, the tuning parameters giving the best displacement estimates also produced the lowest acceleration error. This behavior, however, may not be true in all scenarios and for all noise levels. To test the assumption that the best acceleration and displacement estimates are produced by the same tuning parameters, various amounts of noise were added to both the system model and the acceleration measurements to see what effects, if any, they had on tuning for displacement estimates.

3.3.2 Tuning when model noise and measurement noise is present

Imperfections were added to both the system model used in the dual Kalman filter and the acceleration measurements to determine what effects, if any, the imperfections had on tuning for displacement estimates. Various levels of damping were also considered. For each scenario, the DKF algorithm was implemented assuming a measurement noise covariance of $\mathbf{R} = 10^{-7} \times \mathbf{I}$. Displacement estimates were generated over the range $Q^x = [10^{-20}, 10^{-5}]$ and $Q^p = [10^{-20}, 10^{0}]$, and the acceleration error and displacement error surfaces were analyzed in an attempt to correlate the displacement estimate quality with the acceleration estimate quality.

3.3.2.1 Model noise – natural frequencies and mode shapes

Model noise was introduced using noisy natural frequencies and mode shapes (i.e., natural frequencies and mode shapes that were different from the parameters of the true system in Section 3.2) in the development of the DKF equations. The level of noise under consideration was motivated by the variation seen in the system identification results of the I-35W Saint Anthony Falls Bridge (Gaebler et al. 2018). Variation of the modal parameters identified for the I-35W Saint Anthony Falls Bridge was seen in two forms: in the range of the identification results over a short time period (i.e., less than one month) and in the seasonal variation of the identification results with a period of one year. Both forms of variation were modeled in the simulated system. The spread in the identification results of the I-35W Saint Anthony Falls Bridge over a short time period of three weeks was modeled using the mode shapes and natural frequencies given in Figure 6 and Table 1, respectively, and was labeled as the "noisy" model. The seasonal variation in natural frequencies seen in Gaebler et al. (2018) for the I-35W Saint Anthony Falls Bridge was modeled using natural frequencies 0.105 Hz higher than those used in the noisy model and using the same mode shapes as the noisy model.

The amount of noise added to the modal properties of the system made no difference in any aspect of the tuning procedure or estimate quality. Figure 7 shows the acceleration and displacement error over the range of Q^x and Q^p for the noisy system model with perfect measurements. The tuning surfaces of the models containing the two magnitudes of noise appeared similar in shape and magnitude to those constructed with the true modal properties, and the best displacement estimates ($Q^x = 10^{-15}, Q^p = 10^{-6}$) were able to capture the true system response. The best displacement estimates were generated by the tuning parameters that also produced the best acceleration estimates.

3.3.2.2 Damping

The effect of damping on tuning for displacement estimates was considered in two ways: (1) by varying the magnitude of the damping ratio over the range $0.5\% \leq \zeta \leq 10\%$ and (2) by using a poor-quality damping identification in the dual Kalman filter estimation system model.

The response of the system was simulated for true modal damping of 0.5%, 2%, and 10%, and tuning surfaces were generated assuming a system model constructed using the true damping values. Each scenario was under the same excitation, and therefore the magnitude of the response decreased with increased damping. The acceleration and displacement error over the range of Q^x and Q^p for the 0.5% and 10% modally damped cases are shown in Figure 8 and Figure 9, respectively. The 2% modally damped error metrics are shown in Figure 4. Because the two error metrics were not normalized, the error values obtained for the three damping cases are not directly comparable. Comparison of Figure 4, Figure 8, and Figure 9 show that while different in magnitude, the shapes of the error surfaces for the different levels of damping had similar characteristics. The flat regions on the displacement error surfaces that yielded essentially the same displacement estimate could be identified by the flat areas on the acceleration error surface; however, the values of the tuning parameters contained within each of the flat regions changed slightly with changes to system damping. For all the trial damping ratios, tuning values near the flat region produced by low values of Q^x and high values of Q^p provided the best displacement and acceleration estimates. Table 2 lists the tuning parameters which yielded the best displacement estimates for each level of damping. The magnitude and frequency content of the true system response was captured by the dual Kalman estimator for all of the considered levels of damping.

Accurate identification of structural damping is often the most difficult component of system identification. Poor damping identification was simulated by assuming 5% modal

damping in the dual Kalman filter system when the acceleration measurements were generated from a 2% modally damped system. The acceleration and displacement error surfaces are shown in Figure 10 for the poor damping identification case. Generally, the error surfaces were similar in shape to those for which the assumed damping matched the level of damping used to generate the acceleration measurements. The tuning parameters that yielded the lowest displacement error are compared to the tuning parameters for other damping cases in Table 2. Even though the level of damping used in the dual Kalman filter system model overpredicted the level of damping in the true system, the magnitude and frequency content of the true system response was captured by the dual Kalman estimator.

For the damping cases considered in this study, results indicated that (1) for the range of damping values typically exhibited by large structures, similar tuning values produced the same relative quality of displacement estimate and (2) good displacement estimates could be recovered using poor identification results assuming the measurements were of similar quality to those taken from the I-35W Saint Anthony Falls Bridge. In addition, the best displacement estimates were generated by the tuning parameters that also produced the best acceleration estimates.

3.3.2.3 Model truncation

As the development of the dual Kalman filter was suitable for model constructions using only a few modes, the effect of model truncation was considered by generating estimates using only the first four modes of the system model presented in Section 3.2. As would be expected, truncating the model diminished the estimator's capability to capture the exact, full order response to a white noise excitation. Figure 11 shows a portion of the best displacement estimate time history for a truncated model with noisy modal parameters and 2% damping. Similar to the best tuning parameters for the full order model, the tuning values that provided the best displacement estimates for the truncated model ($Q^x = 10^{-14}, Q^p = 10^{-7}$) were near the flat region on the acceleration error tuning surface produced by low values of Q^x and high values of Q^p. The shapes of the error surfaces were similar between the truncated and full order model, and the best displacement estimates were produced by the tuning parameters that gave the best acceleration estimates.

3.3.2.4 Measurement noise

Measurement noise was introduced to the 0.5%, 2%, and 10% damped systems by adding a zero-mean Gaussian noise to the simulated acceleration responses. Various signal-to-noise

ratios (SNR) were considered (SNR = 15, 20) to simulate the noise levels seen in the accelerometer data obtained from the I-35W Saint Anthony Falls Bridge (French et al. 2012). The dual Kalman filter algorithm was implemented assuming the true full order model presented in Section 3.2 with measurement noise covariance $\mathbf{R} = 10^{-7} \times \mathbf{I}$.

For both noise levels (SNR = 15, 20) and all damping levels (0.5%, 2%, and 10%), the shape of the acceleration error surface was like all other cases; however, the displacement error surface shape was different than the displacement error surfaces generated with no measurement noise. Figure 12 shows the acceleration and displacement error for the 2% damped system with measurement noise (SNR = 20). The surface was shown from a different perspective so the point with the minimum displacement error was visible ($Q^x = 10^{-13}, Q^p = 10^{-12}$). Unlike all other forms of model noise considered, the minimum error displacement estimates were not generated by the tuning parameters that produced the minimum error acceleration estimates. Instead of the minimum error displacement estimates being generated by tuning parameters near the flat region on the acceleration error tuning surface corresponding to low values of Q^x and high values of Q^p, the minimum error displacement estimate for a system with measurement noise was generated from tuning parameters with relatively high assumed process noise Q^x and low assumed input noise Q^p. A portion of the displacement estimate at node 4 produced by the minimum error tuning parameters is shown in Figure 13. Significantly poorer displacement estimation performance was achieved when measurements were contaminated with noise as compared to cases with no measurement noise.

The shape differences of the acceleration error and displacement error tuning surfaces for the case with significant measurement noise suggested that the tuning parameters which produce the minimum error displacement estimates cannot be identified from the acceleration error tuning surface alone.

3.4 Tuning conclusions

A simulated 8 degree of freedom system was considered to assess an expanded L-curve-type tuning approach for displacement estimation from acceleration measurements using the dual Kalman filter. The expanded tuning approach incorporated parameters that reflect the unknown process noise and input noise of the estimation system (Q^x and Q^p, respectively).

A tuning surface of the acceleration estimate error vs Q^x and Q^p was generated and compared to the displacement estimate error to study the relationship between the optimal tuning parameters for the observed and unobserved quantities. Several cases of model and measurement noise were considered; and for systems with similar modal properties to the I-35W Saint Anthony Falls Bridge, results showed that modeling errors due to poor identification results had less of an effect on the tuning procedure than measurement error. Because of measurement error, the tuning parameters that generated minimum error displacement estimates could not be selected from the acceleration error tuning surface alone.

Generally, the acceleration error surface can be used to define a region of tuning parameters that make a difference on the displacement and velocity estimates. The estimates produced by this region of tuning parameters must then be inspected to select the proper tuning parameters that provide an acceptable displacement estimate. When implemented on civil structures in the field, engineering judgment must be used to select the tuning parameters. From experimentation on the simulated 8 degree of freedom system, often the best choice of tuning parameters was one which produced displacement estimates that had the largest peaks while remaining smooth.

Chapter 4: Blind case study

To test the tuning procedure outlined in Chapter 3 for displacement estimation in a more realistic setting, a blind case study scenario was considered. The only information available to the individual who performed the study was (1) noisy acceleration measurements, (2) geometry of the structure including sensor location, and (3) the first 6 natural frequencies of the system. In general, knowledge of the structure geometry and sensor locations are not necessary to implement the dual Kalman filter procedure, but they are usually known. Natural frequency approximations are sometimes available from finite element models and can be used as a check for output-only modal parameter identification.

The blind case study structure is shown in Figure 14 and was designed to roughly approximate a bridge with a flexible pier at midspan. The system modeled a 20 foot long simply supported concrete beam (w_c = 100 lb/ft^3 (15.7 kN/m^3), f_c' = 5 ksi (34 MPa), E_c = 4030.5 ksi (27996 MPa)) with a vertical spring support (k = 441.685 kip/ft (6445.91 kN/m)) at midspan. The rectangular cross section (2 ft (0.6096 m) wide by 6 ft (1.8288 m) deep) was constant along the length of the beam. Table 3 lists the true modal parameters of the system. The simulated system was excited along the length by a spatially correlated band-limited white noise and the corresponding acceleration measurements provided to the user contained measurement noise (SNR = 20).

NExT-ERA/DC (James III et al. 1995; Juang and Pappa 1985; Juang et al. 1988) was used to identify the modal parameters such as natural frequencies, mode shapes, and damping ratios of the unknown system from six separate simulated acceleration data files. For each run, the results were sorted by mode shape, and the identification result with the highest consistent-mode indicator (CMI) was kept (Pappa et al. 1993). Table 4 lists the average modal parameters identified from the six acceleration measurement files provided to the author. These parameters were used to formulate a model of the structure to be used in the dual Kalman filter. The first, third, and fifth vibrational modes of the structure (from Table 3) were identified using the output-only technique.

Figure 15 shows the acceleration error as a function of process noise and input noise covariances for an assumed $\mathbf{R} = \mathbf{I}$. The acceleration error tuning metric provided little guidance in selecting the tuning parameters, so the displacement estimates themselves were assessed. Of

the displacement estimates generated over the range of tuning parameters shown in Figure 15, Figure 16 displays a representative sample of the smoother estimated time histories at node 3. Displacement estimates with large amounts of drift or with frequency content higher than expected were discarded based on engineering judgement. The estimates in Figure 16 differ mainly by the magnitude of the peaks, and those with very low magnitudes have a slight phase shift.

The dashed line ($Q^x = 10^{-7},\ Q^p = 10^{-10},\ \mathbf{R} = \mathbf{I}$) in Figure 16 was a smooth estimate (essentially no visible high frequency content) with peak magnitudes that encompass all other peaks. Towards the end of the acceleration record, this dashed estimate drifts slightly away from an estimate with a true zero mean and more high frequency content. If a truly smooth estimate without drift was desired, the dashed line could be used to estimate shorter segments of data, thus avoiding the drift that occurs after long periods of time. However, the effects of the filter initial conditions must be considered if taking such an approach. An estimate with similarly large peak amplitudes, but with a low level of high frequency content ($Q^x = 10,\ Q^p = 10^{-6},\ \mathbf{R} = \mathbf{I}$) was selected instead of the dashed estimate as the authors' "best guess" for displacement estimation. Selecting the estimate with the largest magnitude was treated as a conservative approach, especially if large displacements were unfavorable. Figure 17 shows the input estimates at node 3 corresponding to the two displacement estimates previously mentioned ($\{Q^x = 10^{-7},\ Q^p = 10^{-10}\}$ and $\{Q^x = 10,\ Q^p = 10^{-6}\}$). In comparing the estimated inputs, significant drift in the input estimation appears to cause the slight drift in the dashed displacement estimate.

After the tuning parameters ($Q^x = 10, Q^p = 10^{-6},\ \mathbf{R} = \mathbf{I}$) were chosen and the system response was estimated, the true displacements were revealed to the author performing the blind analysis. Figure 18 shows the estimated displacements compared to the true displacements at node 3 for a single run. In this case, there was good agreement between the estimated and true displacements (node 3 RMSE = 0.0201 inches (0.5105 mm)). These results indicate that the tuning procedure outlined in Section 3 can provide acceptable displacement estimates in a field setting.

Chapter 5: Advantages of the dual Kalman filter when inputs are not of interest

In this work, the input estimator in the dual Kalman filter was used as a tool towards state estimation. The main reason for the use of the dual Kalman filter, rather than a single Kalman filter, was improved displacement estimation performance, especially under various loading types. When no input estimator is used, an assumption on the type of excitation is necessary. If the loading assumption is incorrect, significant filter performance degradation may be observed. The increased performance of the dual Kalman filter over the single Kalman filter in instances with unknown loading is explored in the following sections via a simulated example and an experimental test.

5.1 Simulated example

For the simulated example, state estimation of the 8-DOF system with 2% damping in Chapter 3 was considered using a single Kalman filter (Kalman 1960). The system was excited by a random white noise excitation at all nodes, but randomly shifted in time. The estimation problem was formulated using Eq. (10) and setting $\mathbf{B}_\mathrm{d} = \mathbf{0}$ and $\mathbf{D}_\mathrm{d} = \mathbf{0}$. Such a construction inherently assumed that the modal excitation is a zero mean white noise. For comparison of the two formulations, i.e. a single Kalman filter (with $\mathbf{B}_\mathrm{d} = \mathbf{0}$ and $\mathbf{D}_\mathrm{d} = \mathbf{0}$) and the dual Kalman filter, the modal parameters used in the dynamic models were exact, and no measurement noise was added.

Figure 19 shows a portion of the most accurate displacement estimate time histories for the single Kalman and dual Kalman estimation methods for the 8-DOF system under random loading. The single Kalman filter estimates (Displacement Error = 0.008211 m) were not as accurate as the dual Kalman filter estimates (Displacement Error = 0.001543 m), but the single Kalman filter did give reasonable displacement estimates for some portions of the time history. The tuning parameters that generated the best displacement estimate were not the same for the single Kalman estimator ($Q^x = 10^{-13}$) and dual Kalman estimator ($Q^x = 10^{-16}, Q^p = 10^{-7}$). Figure 20 shows the acceleration and displacement error for the single Kalman filter estimates as a function of Q^x. Even though the single Kalman filter could match the acceleration

measurements to a high precision for increasing Q^x in Figure 20a, increased acceleration estimate accuracy did not reduce the displacement estimate error seen in Figure 20b.

Higher accuracy was not achieved in the single Kalman filter displacement estimates by using a process noise covariance of $Q^x = 2.8657$, i.e. the true covariance of the random excitation. With the process noise covariance assumed known, the measurement noise covariance was varied as the single tuning parameter of the system and the best displacement estimates were generated by the noise covariance parameters $Q^x = 2.8657$ and $\mathbf{R} = 10^6 \times \mathbf{I}$ (Displacement Error = 0.008274 m). The process noise and measurement noise covariance combinations generated similar state estimates because the two ratios of process noise to measurement noise were similar. The ratio-dependence of the Kalman-type filters, instead of each noise covariance parameter influencing the filter independently, was also observed by previous researchers (Auger et al. 2013; Bittanti and Savaresi 2000).

Although the two Kalman filter implementations can be effective for the modified random excitation used in the simulated case study, a single Kalman filter was not able to capture the initial displacement response in the case of an impulse loading. An impulse time history with a single nonzero value of 1000 at $t = 1\ sec$ was applied to node 4 of the same 8-DOF model with 2% damping described in Chapter 3. The system response was estimated using both the single and dual Kalman filter estimators. From the possible range of estimates, the best displacement estimates were generated with the same noise covariances as for the random excitation case and are shown in Figure 21. The dual Kalman filter was able to react faster than the single Kalman filter to the acceleration measurements while remaining smooth. This behavior was observed in the single Kalman filter estimates because the impulse loading violated the assumption of a Gaussian white noise excitation. However, the single Kalman filter displacement estimates were nearly identical to the dual Kalman filter estimates and the true displacement response starting about 1.1 seconds (110 measurements) after the impulse. The speed with which the single Kalman filter approaches the dual Kalman filter is dependent on the selection of Q^x and $\mathbf{R}$. As more trust was placed in the measurements, the initial spike in the single Kalman estimator increased in magnitude but corrected to the true value quicker.

5.2 Experimental test

To verify the proposed dual Kalman filter estimation technique on a physical structure, a small-scale laboratory test was conducted in the Theodore V. Galambos Structural Engineering Laboratory at the University of Minnesota that compared displacements estimated using the Kalman filtering technique to displacements measured using linear variable differential transformers (LVDTs). The laboratory test was performed on a single-story, single-bay steel frame with bolted connections. Figure 22 shows the experimental set up. An HSS 6x6x3/8 test beam was suspended between two W12x120 columns, and an isolated wooden frame was built beside the test frame as a reference platform for the LVDTs. For the experimentation discussed here, the actuator connected to the test beam in Figure 22 was disconnected; instead, excitation was supplied using a padded sledge hammer.

The test beam was subjected to an impact force, and the subsequent acceleration and displacement response was measured at eight locations along the beam. LVDTs measured displacements at the locations of the accelerometers. Figure 23 shows a schematic drawing of the experimental setup and sensor locations. Figure 24 shows the accelerometer and LVDT attachment. At each sensing location, a PCB Piezotronics model 352C33 piezoelectric shear accelerometer (100 mV/g) and a $\pm$0.5" Schaevitz LVDT were fastened to an aluminum angle that was glued to the test beam. Data was collected using an NI cDAQ-9178 and was sampled at 1600 Hz. The signals were passed through an elliptic low-pass filter with a 400 Hz cutoff frequency.

Displacements were estimated at the locations of the accelerometers using single and dual Kalman filter estimation techniques, and the estimated displacements were compared to the measured displacements. The system model was constructed using modal parameters determined from the output-only system identification technique ERA/DC (Juang et al. 1988). The identified modal parameters for the steel beam are listed in Table 5. The measurement noise covariance matrix **R** was assumed to be the identity matrix of appropriate dimension for both the single and dual Kalman filters. Similar to previous filter constructions, the coefficients on the process noise covariance matrix (for the single and dual Kalman filter) and input noise covariance matrix (dual Kalman filter only) were treated as the tuning parameters of the two systems. The best tuning parameters were selected as those which produced displacement estimates most closely matching the measured displacements using the displacement error metric introduced in Section 3.

The displacement estimation results at location 4 (nearest midspan) are shown in Figure 25 for the single and dual Kalman filter approaches and compared to the measured response. Like

the simulated example, the dual Kalman filter was able to match the true displacement response due to an impact load faster than the single Kalman approach. However, the dual Kalman filter displacement estimates spike immediately following the impact. The initial large peak is likely non-physical due to the response time of the system. The first oscillatory peak, which would be the largest, is captured by the dual Kalman filter and not the single Kalman filter. The initial magnitude discrepancy between the measured deflections and those estimated using the single Kalman filter are attributed to the incorrect, built-in assumption of random loading. As such, the single Kalman filter was not well suited to estimate sudden displacement changes due to a large change in loading.

Chapter 6: Conclusions

This work explored a tuning procedure for the output-only implementation of the dual Kalman filter for displacement estimation via noisy acceleration measurements. The tuning process was an expanded L-curve approach for proper selection of two noise covariance parameters describing the unknown input and process noise of the system. Given that the actual displacement response of the structure was unavailable, selecting optimal tuning parameters based on a displacement error metric was impossible. Therefore, an acceleration-based metric was used to generate a range of possible tuning parameters, then engineering judgement was used to evaluate the true response of the structure.

The tuning procedure was demonstrated on a simulated system reflecting the vibrational response characteristics of the I-35W Saint Anthony Falls Bridge, a simulated blind case study system modeling a simply supported concrete beam with a flexible pier at midspan, and a laboratory experiment on a full-scale steel beam. Good dynamic displacement estimates were achieved for all cases using the dual Kalman filter. The approach indicated that model noise (e.g., due to poor system identification results) did not affect the tuning process as much as measurement noise. Additionally, the output-only formulation of the problem without structural mass information required that modal participation factor approximations be made, and thus caused the unknown input estimates to lose physical meaning. Despite these caveats, the input estimator significantly increased state estimation performance under various loading types as compared to a single Kalman filter.

Tables

Table 1: Natural frequencies (Hz) for simulated 8-DOF clean and noisy model.

Mode	1	2	3	4	5	6	7	8
Clean	0.78	1.54	2.25	2.89	3.45	3.90	4.23	4.43
Noisy	0.77	1.56	2.28	2.87	3.45	3.91	4.21	4.38

Table 2: Best tuning parameters for simulated 8-DOF systems with various levels of damping.

Damping		Parameters giving best displacement estimates	
True	Assumed	Q^x	Q^p
0.5%	0.5%	10^{-17}	10^{-6}
2%	2%	10^{-16}	10^{-6}
10%	10%	10^{-16}	10^{-6}
2%	5%	10^{-15}	10^{-6}

Table 3: True modal properties of blind case study system.

Mode	Natural Frequency	Damping Ratio	Mode Shape							
[]	[Hz]	[]	dof 1	dof 2	dof 3	dof 4	dof 5	dof 6	dof 7	dof 8
1	3.06	0.02	0.35	0.65	0.88	1	1	0.88	0.65	0.35
2	4.46	0.025	0.65	1	0.88	0.35	-0.35	-0.88	-1	-0.65
3	9.89	0.03	1	1	0	-1	-1	0	1	1
4	17.84	0.031	1	0.35	-0.88	-0.65	0.65	0.88	-0.35	-1
5	27.90	0.04	1	-0.35	-0.88	0.65	0.65	-0.88	-0.35	1
6	40.14	0.06	1	-1	0	1	-1	0	1	-1

Table 4: Identified modal properties of blind case study system. Standard deviation of identification results in parenthesis.

Identified Mode	Natural Frequency	Damping Ratio	Mode Shape							
[]	[Hz]	[]	dof 1	dof 2	dof 3	dof 4	dof 5	dof 6	dof 7	dof 8
1	3.07 (0.05)	0.030 (0.005)	0.32 (0.03)	0.63 (0.02)	0.86 (0.01)	1.00 (0.01)	1.00 (0.01)	0.86 (0.01)	0.62 (0.02)	0.32 (0.03)
2	9.88 (0.06)	0.027 (0.007)	0.88 (0.01)	0.85 (0.01)	-0.08 (0.01)	-1.00 (0.01)	-1.00 (0.01)	-0.08 (0.01)	0.85 (0.01)	0.88 (0.01)
3	27.81 (0.36)	0.024 (0.005)	0.98 (0.03)	-0.35 (0.04)	-0.87 (0.04)	0.64 (0.02)	0.69 (0.05)	-0.86 (0.02)	-0.38 (0.07)	1.00 (0.01)

Table 5: Identified modal properties of steel beam.

Identified Mode	Natural Frequency	Damping Ratio	Mode Shape							
[]	[Hz]	[]	dof 1	dof 2	dof 3	dof 4	dof 5	dof 6	dof 7	dof 8
1	24.5	0.002	0.43	0.66	0.93	1.00	0.92	0.38	0.99	0.99
2	90.9	0.017	0.83	1.00	0.78	0.31	-0.55	-0.57	-0.14	-0.15
3	173.8	0.007	0.99	0.86	0.06	-0.45	0.12	1.00	-0.35	-0.37
4	282.3	0.013	0.90	0.04	-1.00	-0.58	0.58	-0.87	0.18	0.20

Figures

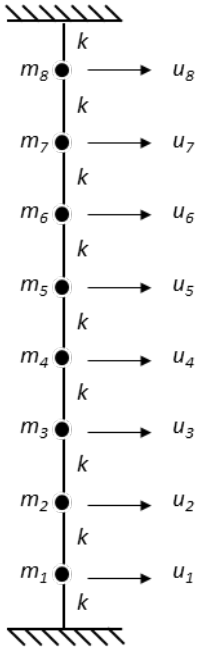

Figure 1: Simulated 8 degree of freedom system.

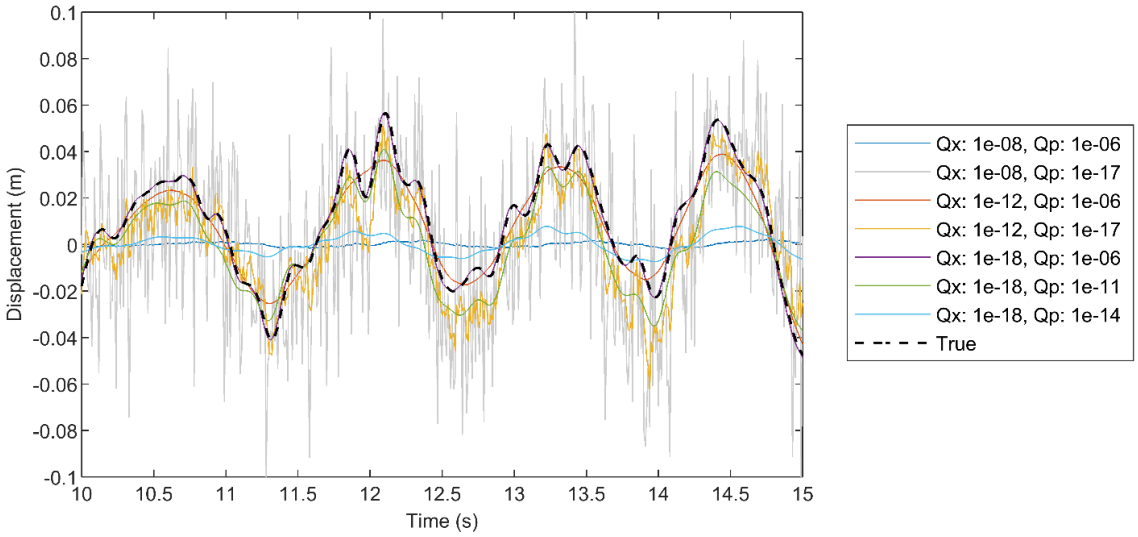

Figure 2: Displacement estimate range at node 4 of 8-DOF system. Clean model, clean measurements, 2% damping.

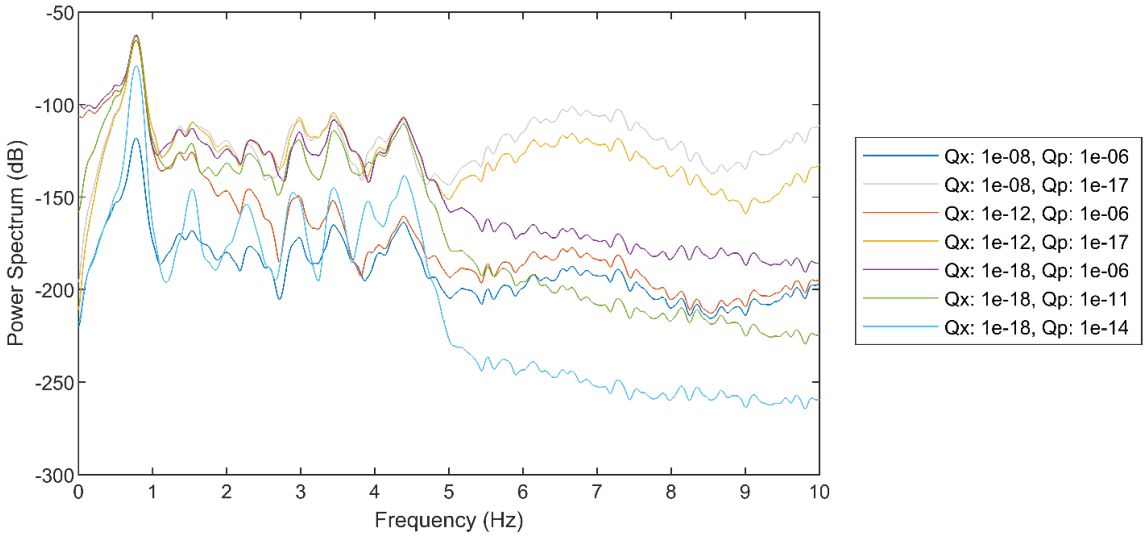

Figure 3: Power spectrum of 8-DOF system displacement estimates. Clean model, clean measurements, 2% damping.

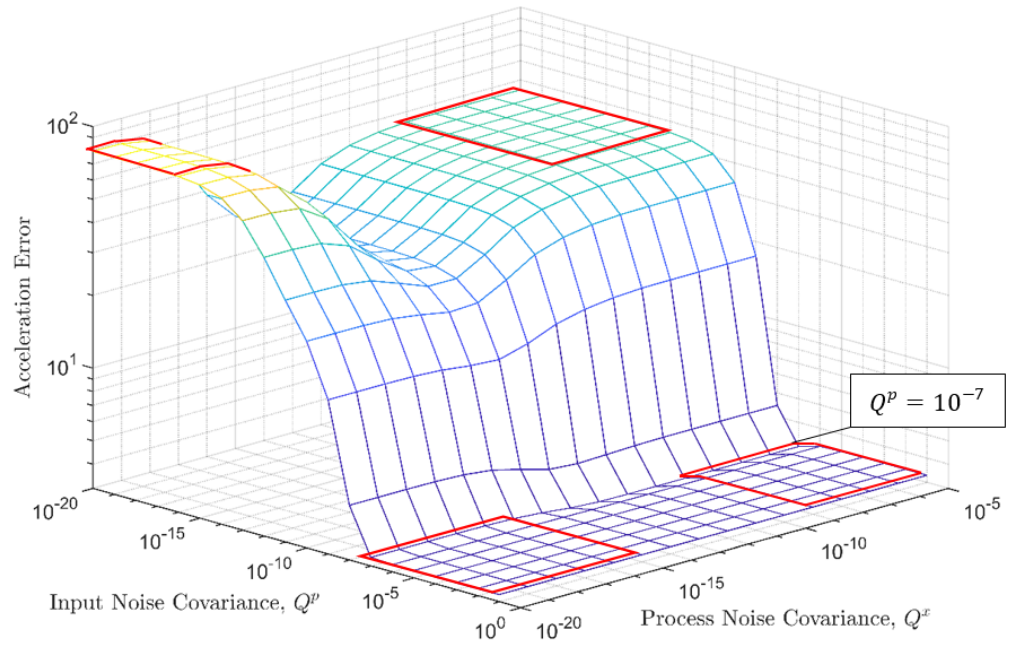

Figure 4a: Acceleration estimation error surface for 8-DOF system. Clean model, clean measurements, 2% damping.

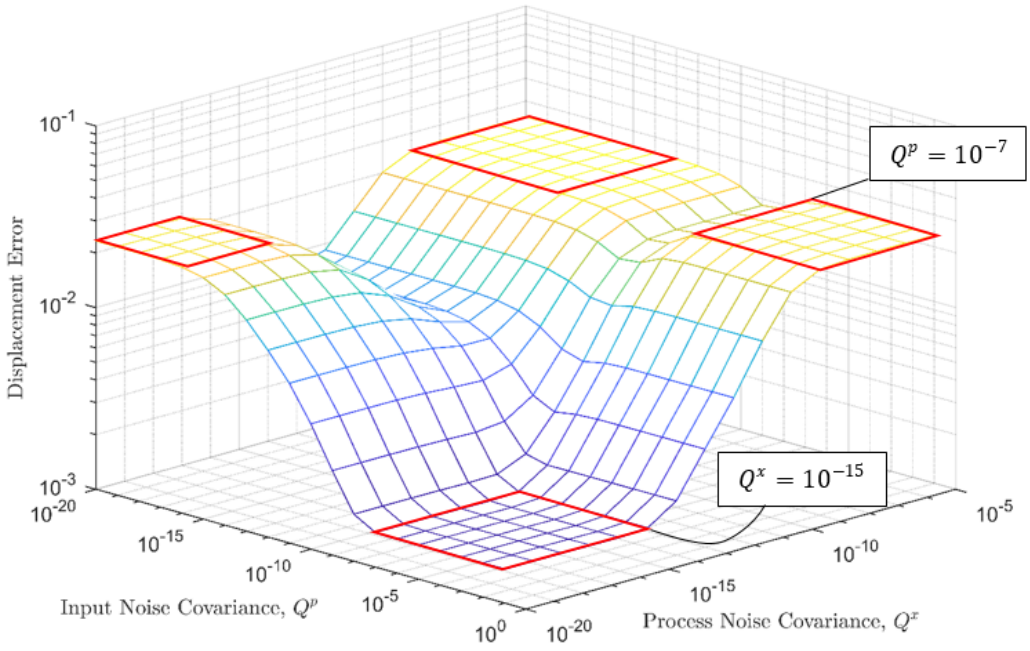

Figure 4b: Displacement estimation error surface for 8-DOF system. Clean model, clean measurements, 2% damping.

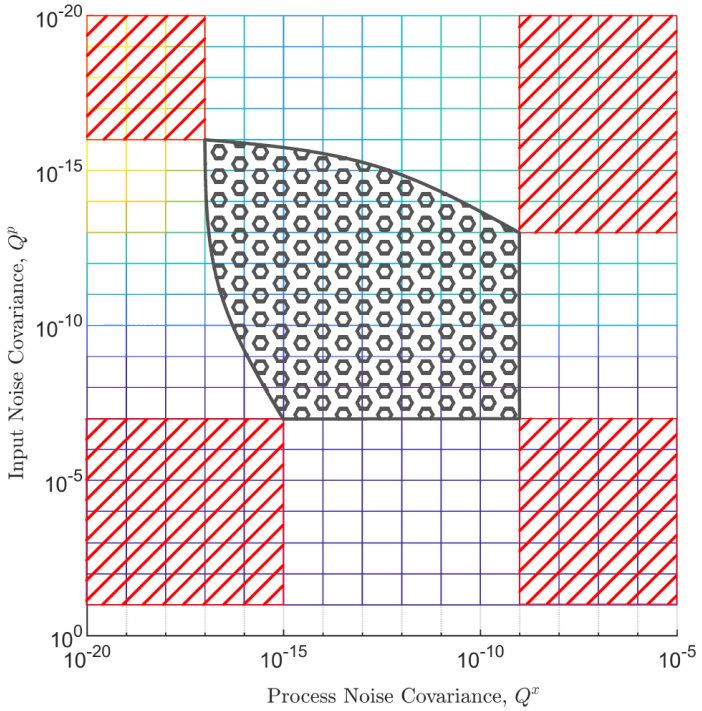

Figure 5: Top-down view of acceleration error surface in Figure 4a. Flat regions (diagonal hatch) identify a region of tuning parameters that generate all possible displacement estimates (hexagon hatch).

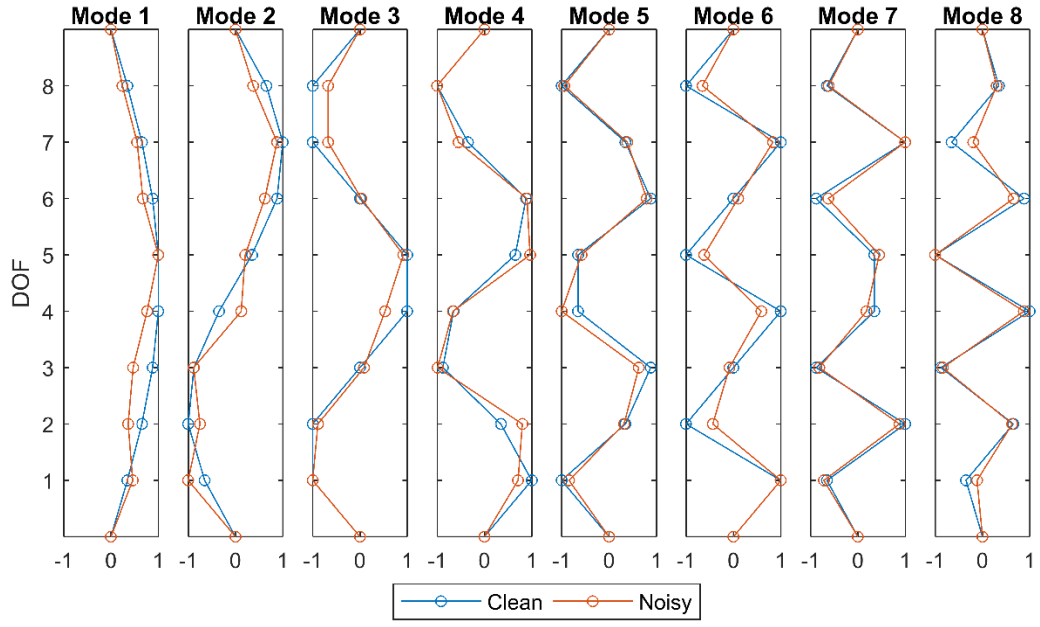

Figure 6: Mode shapes for 8-DOF clean and noisy model.

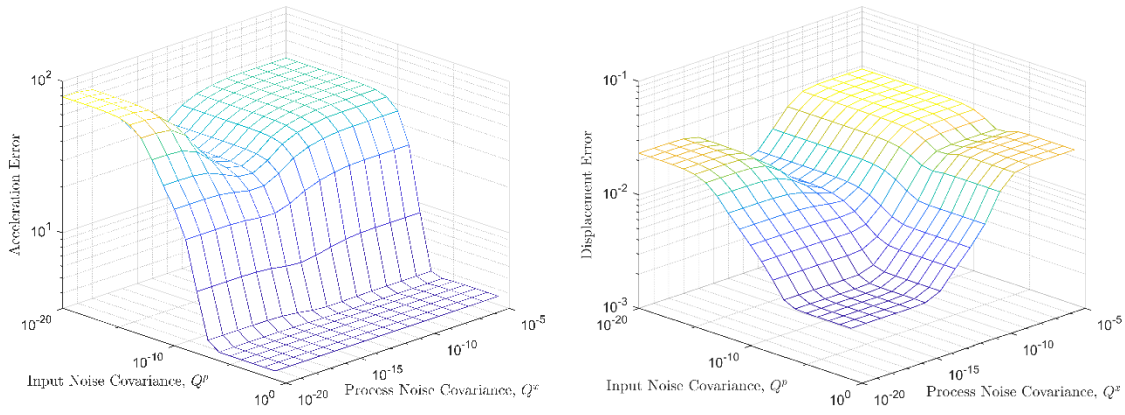

Figure 7: (Left) Acceleration and (right) displacement estimation error surface for 8-DOF system. Noisy model, clean measurements, 2% damping.

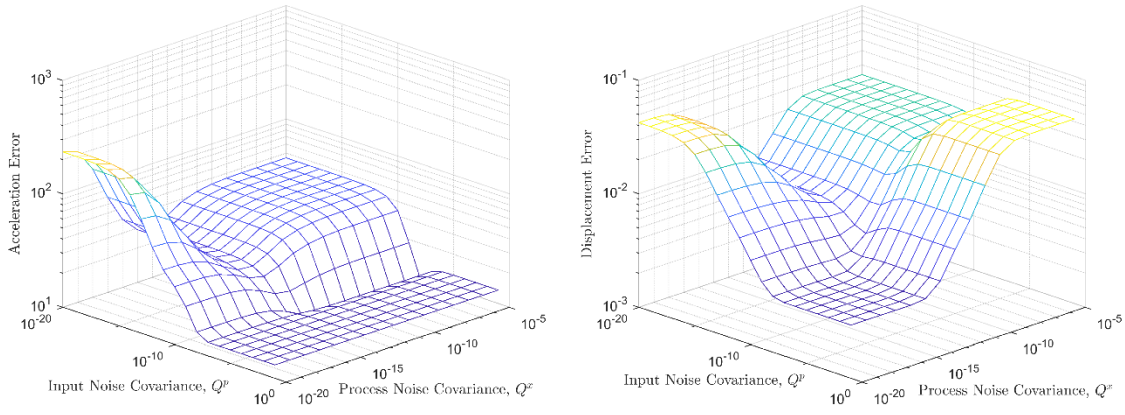

Figure 8: (Left) Acceleration and (right) displacement estimation error surface for 8-DOF system. Clean model, clean measurements, 0.5% damping.

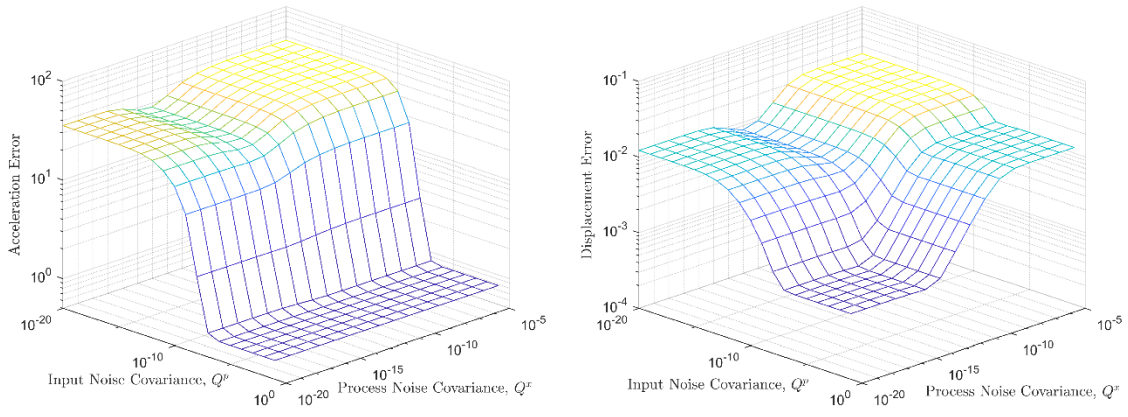

Figure 9: (Left) Acceleration and (right) displacement estimation error surface for 8-DOF system. Clean model, clean measurements, 10% damping.

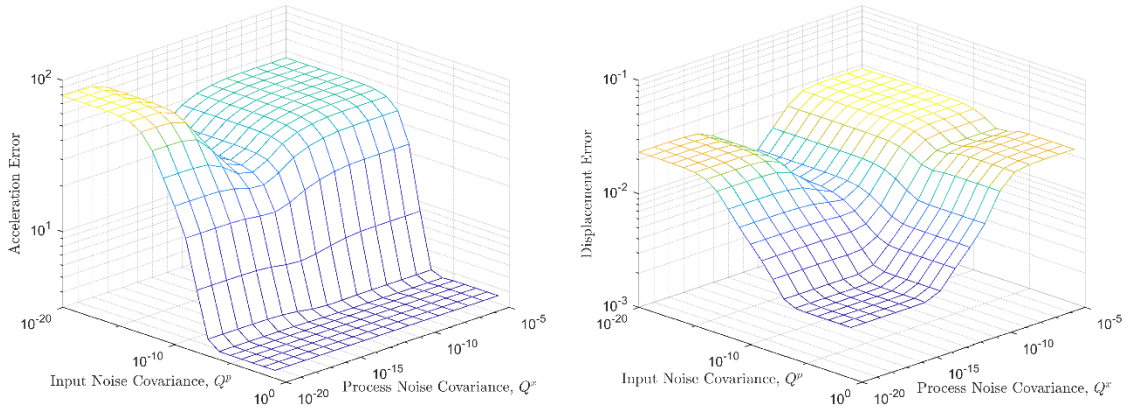

Figure 10: (Left) Acceleration and (right) displacement estimation error surface for 8-DOF system. Clean model, clean measurements generated from 2% damping model, assumed 5% damping for DKF implementation.

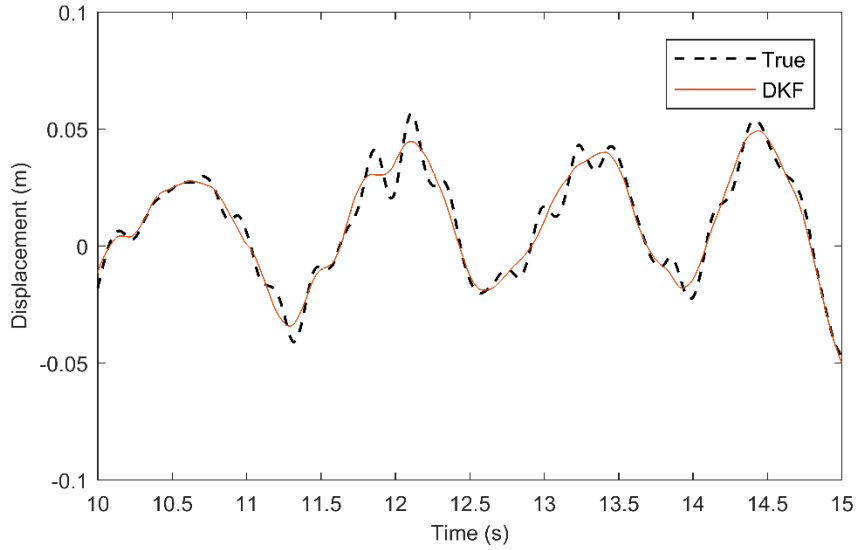

Figure 11: Displacement estimate of 8-DOF system at node 4. Truncated model, clean measurements, 2% damping.

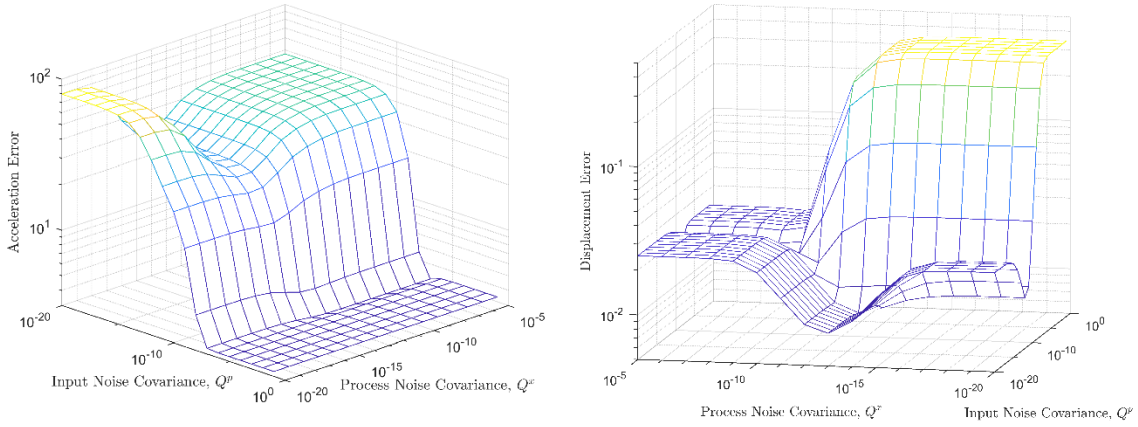

Figure 12: (Left) Acceleration and (right) displacement estimation error surface for 8-DOF system. Clean model, noisy measurements (SNR = 20), 2% damping.

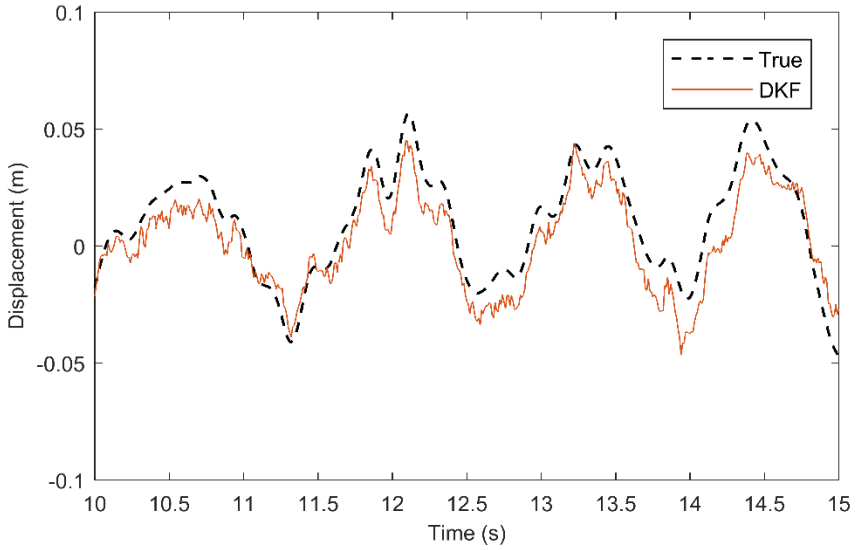

Figure 13: Displacement estimate of 8-DOF system at node 4. Clean model, noisy measurements (SNR = 20), 2% damping.

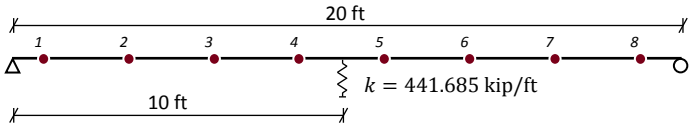

Figure 14: Blind case study system.

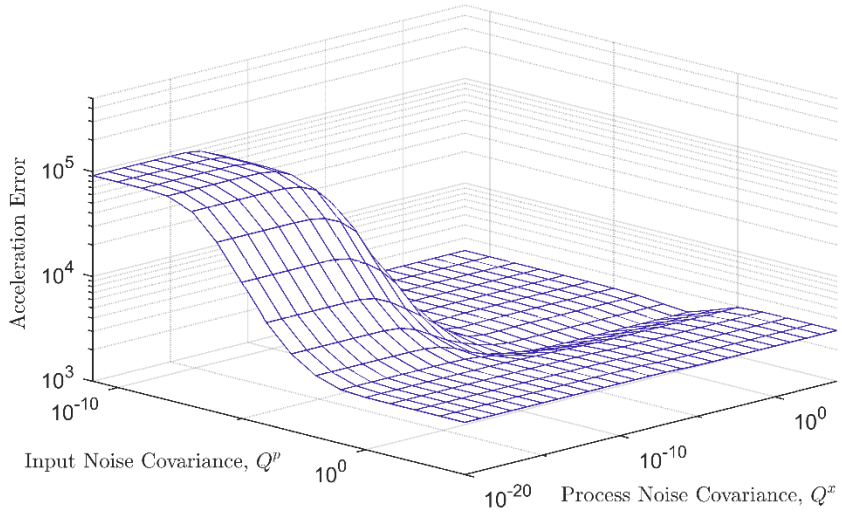

Figure 15: Acceleration estimation error surface for blind case study system.

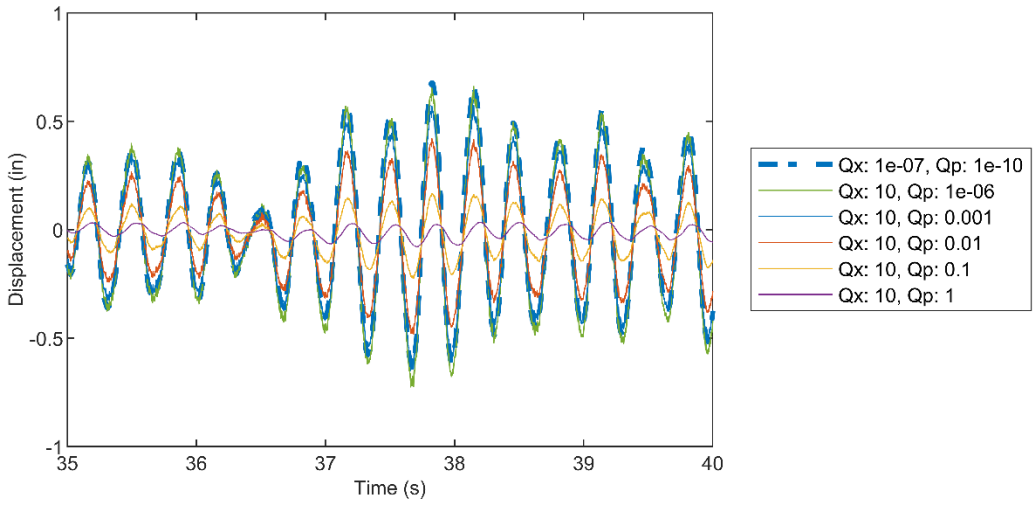

Figure 16: Displacement estimate range at node 3 for blind case study system.

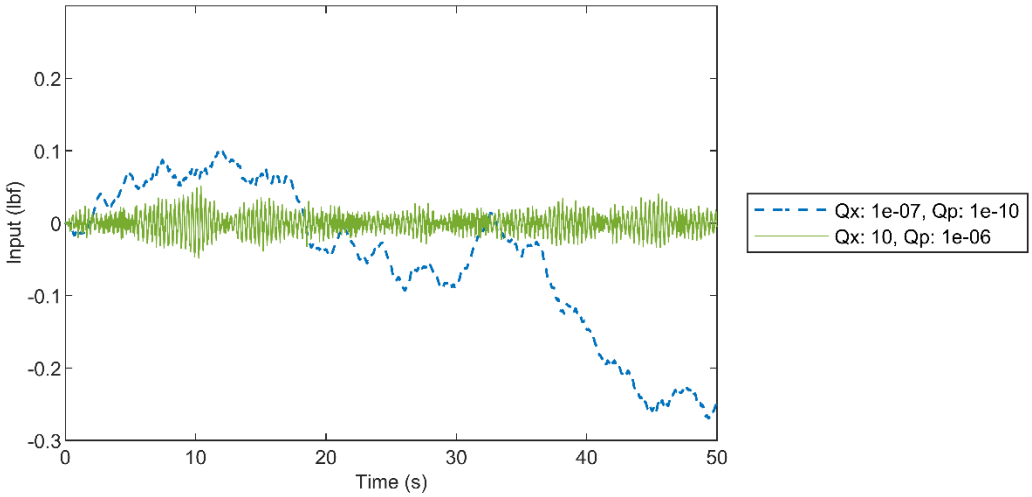

Figure 17: Input estimates at node 3 for blind case study system.

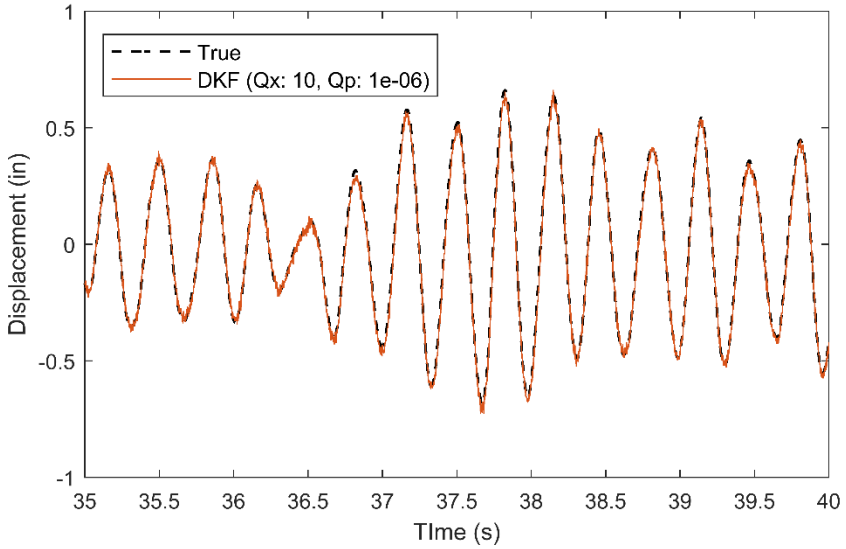

Figure 18: Comparison of displacement estimate from dual Kalman filter (DKF) for blind case study system at node 3.

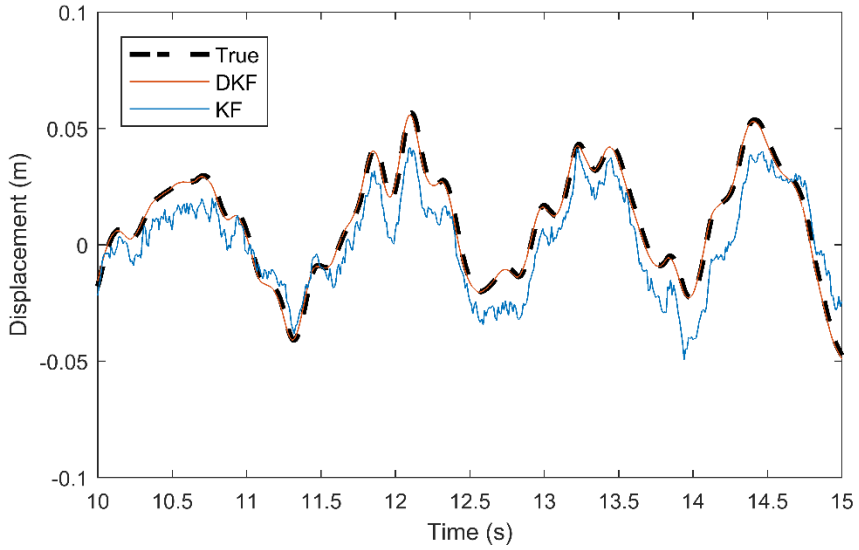

Figure 19: Displacement estimates from dual Kalman filter (DKF) and single Kalman filter (KF) at node 4 for 8-DOF system under random excitation. Clean model, clean measurements, 2% damping.

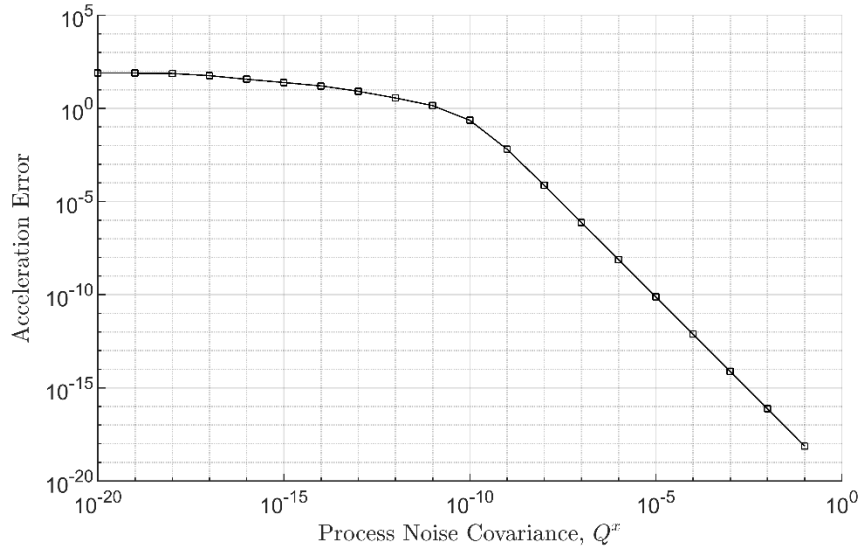

Figure 20a: Single Kalman filter acceleration estimation error for 8-DOF system under random excitation. Clean model, measurements. 2% damping.

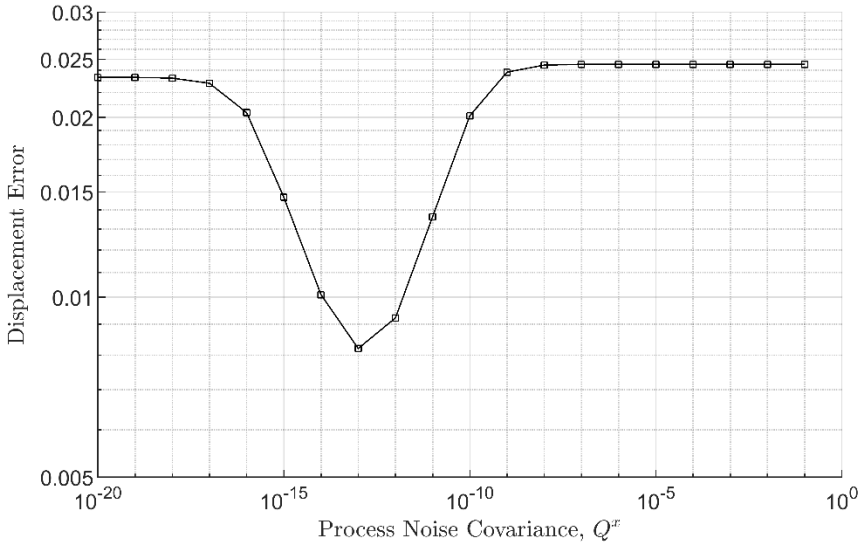

Figure 20b: Single Kalman filter displacement estimation error for 8-DOF system under random excitation. Clean model, measurements. 2% damping.

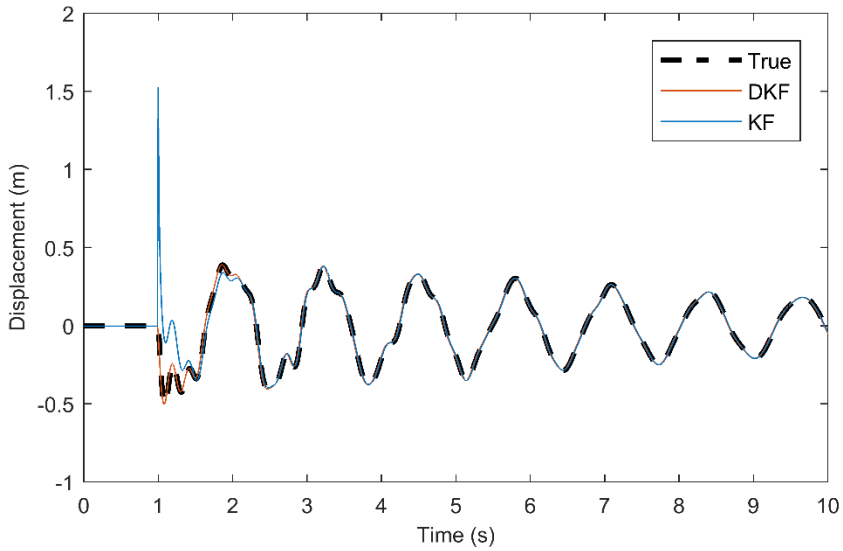

Figure 21: Displacement estimates from dual Kalman filter (DKF) and single Kalman filter (KF) at node 4 for 8-DOF system under impulse excitation. Clean model, clean measurements, 2% damping.

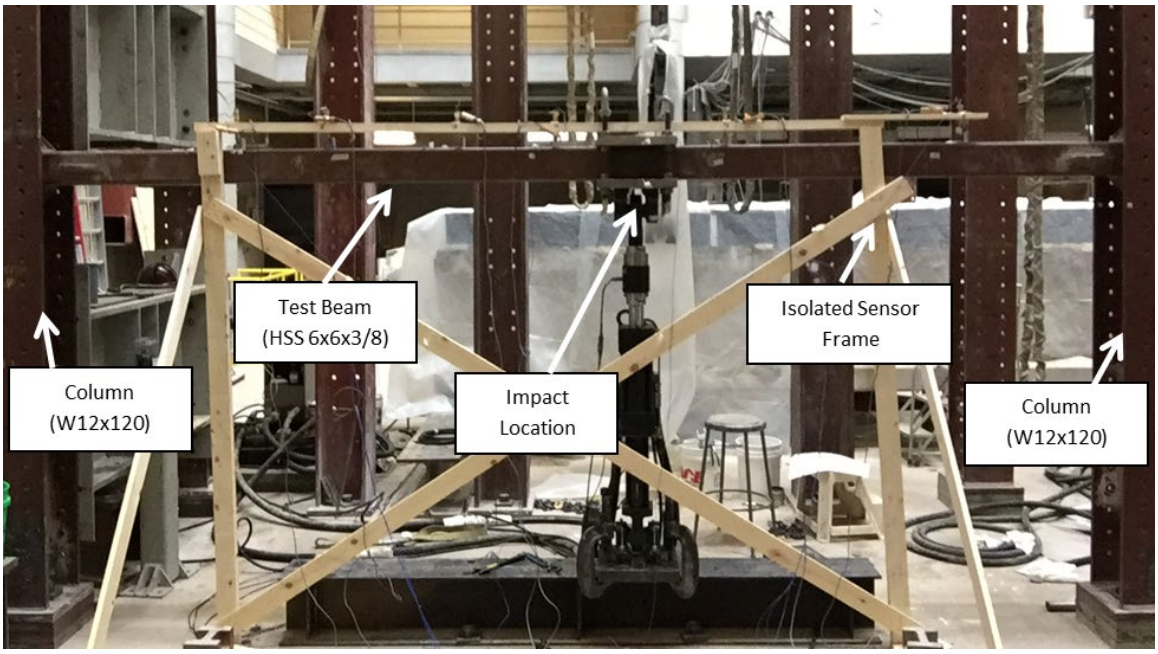

Figure 22: Laboratory set up of experimental steel test beam.

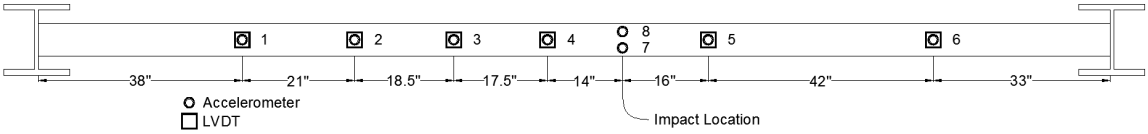

Figure 23: Plan view schematic drawing of experimental setup and sensor locations.

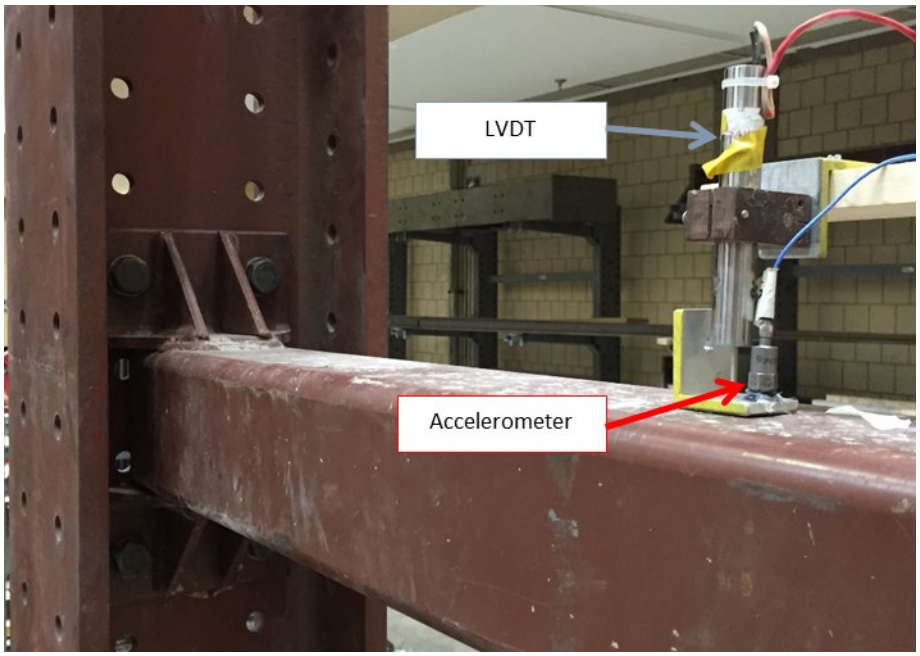

Figure 24: Lab experiment beam-column connection with accelerometer and LVDT attachment.

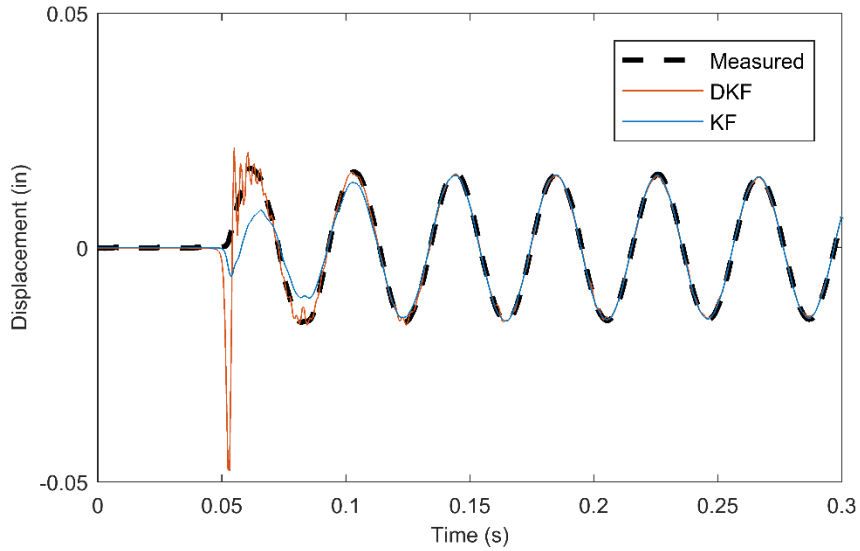

Figure 25: Displacement estimates from dual Kalman filter (DKF) and single Kalman filter (KF) at node 4 for steel beam under impulse excitation.

Bibliography

Auger, F., Hilairet, M., Guerrero, J. M., Monmasson, E., Orlowska-Kowalska, T., and Katsura, S. (2013). "Industrial applications of the kalman filter: A review." *IEEE Transactions on Industrial Electronics*, IEEE, 60(12), 5458–5471.

Bittanti, S., and Savaresi, S. M. (2000). "On the parametrization and design of an extended Kalman filter frequency tracker." *IEEE Transactions on Automatic Control*, 45(9), 1718–1724.

Deraemaeker, A., Reynders, E., De Roeck, G., and Kullaa, J. (2008). "Vibration-based structural health monitoring using output-only measurements under changing environment." *Mechanical Systems and Signal Processing*, 22(1), 34–56.

Duník, J., Straka, O., Kost, O., and Havlík, J. (2017). "Noise covariance matrices in state-space models: A survey and comparison of estimation methods—Part I." *International Journal of Adaptive Control and Signal Processing*, 31(11), 1505–1543.

Eftekhar Azam, S., Chatzi, E., and Papadimitriou, C. (2015a). "A dual Kalman filter approach for state estimation via output-only acceleration measurements." *Mechanical Systems and Signal Processing*, Elsevier, 60, 866–886.

Eftekhar Azam, S., Chatzi, E., Papadimitriou, C., and Smyth, A. (2015b). "Experimental validation of the dual kalman filter for online and real-time state and input estimation." *Conference Proceedings of the Society for Experimental Mechanics Series*, 3(2015), 1–14.

Faulkner, B. C., Barton, F. W., Baber, T. T., and McKeel, W. T. (1996). *Determination of Bridge Response Using Acceleration Data*. FHWA/VA-97-R5. Virginia Dept. of Transportation, Springfield, VA.

Franklin, G. F., Powell, J. D., and Workman, M. L. (1998). *Digital Control of Dynamic Systems*. Addison-wesley, Menlo Park, CA.

French, C. E. W., Shield, C. K., and Hedegaard, B. D. (2014). *Modeling and Monitoring the Long-Term Behavior of Post-Tensioned Concrete Bridges, MN/RC 2014-39*. Minnesota Dept. of Transportation Research Services & Library, St. Paul, MN.

French, C. E. W., Shield, C. K., Stolarski, H. K., Hedegaard, B. D., and Jilk, B. J. (2012). *Instrumentation, Monitoring, and Modeling of the I-35W Bridge, MN/RC 2012-24*. Minnesota Dept. of Transportation Research Services & Library, St. Paul, MN.

Gaebler, K. O. (2017). "Long-Term Vibration Monitoring of the I-35W St. Anthony Falls Bridge." University of Minnesota. Master's Thesis.

Gaebler, K. O., Hedegaard, B. D., Shield, C. K., and Linderman, L. E. (2018). "Signal selection and analysis methodology of long-term vibration data from the I-35W St. Anthony Falls Bridge." *Structural Control and Health Monitoring*, 25(7), 1–15.

Gaebler, K. O., Shield, C. K., and Linderman, L. E. (2017). *Feasibility of Vibration-Based Long-Term Bridge Monitoring Using the I-35W St. Anthony Falls Bridge, MN/RC 2017-01*. Minnesota Dept. of Transportation Research Services & Library, St. Paul, MN.

Gillijns, S., and De Moor, B. (2007). "Unbiased minimum-variance input and state estimation for linear discrete-time systems with direct feedthrough." *Automatica*, 43(5), 934–937.

Gindy, M., Vaccaro, R., Nassif, H., and Velde, J. (2008). "A State-Space Approach for Deriving Bridge Displacement from Acceleration." *Computer-Aided Civil and Infrastructure Engineering*, 23, 281–290.

Hansen, P. C. (1992). "Analysis of discrete ill-posed problems by means of the L-curve." *SIAM Review*, 34(4), 561–580.

James III, G. H., Carne, T. G., Lauffer, P., J., and Lauffer, J. P. (1995). "The Natural Excitation Technique (NExT) for Modal Parameter Extraction From Operating Structures." *The International Journal of Analytical and Experimental Modal Analysis*, 10(4), 260–277.

Juang, J.-N., Cooper, J. E., and Wright, J. R. (1988). "An Eigensystem Realization Algorithm using Data Correlations (ERA/DC) for Modal Parameter Identification." *Control Theory and Advanced Technology*, 4(1), 5–14.

Juang, J.-N., and Pappa, R. S. (1985). "An Eigensystem Realization Algorithm for Modal Parameter Identification and Model Reduction." *J. Guidance*, 8(5), 620–627.

Kalman, R. E. (1960). "A New Approach to Linear Filtering and Prediction Problems." *Journal of Fluids Engineering*, 82(Series D), 35–45.

Kropp, P. K. (1977). *Experimental Study of the Dynamic Response of Highway bridges*. JHRP-77-5 Indiana State Highway Commission, Indianapolis, IN.

Lainiotis, D. G. (1971). "Optimal adaptive estimation: Structure and parameter adaption." *IEEE Transactions on Automatic Control*, AC-16(2), 160–170.

Lee, J. J., and Shinozuka, M. (2006). "A vision-based system for remote sensing of bridge displacement." *Ndt & E International*, Elsevier, 39(5), 425–431.

Lourens, E., Papadimitriou, C., Gillijns, S., Reynders, E., De Roeck, G., and Lombaert, G. (2012a). "Joint input-response estimation for structural systems based on reduced-order models and vibration data from a limited number of sensors." *Mechanical Systems and Signal Processing*, Elsevier, 29, 310–327.

Lourens, E., Reynders, E., De Roeck, G., Degrande, G., and Lombaert, G. (2012b). "An augmented Kalman filter for force identification in structural dynamics." *Mechanical Systems and Signal Processing*, Elsevier, 27(1), 446–460.

Maes, K., Lourens, E., Van Nimmen, K., Reynders, E., De Roeck, G., and Lombaert, G. (2015). "Design of sensor networks for instantaneous inversion of modally reduced order models in structural dynamics." *Mechanical Systems and Signal Processing*, 52, 628–644.

Magalhães, F., Cunha, A., and Caetano, E. (2012). "Vibration based structural health monitoring of an arch bridge: From automated OMA to damage detection." *Mechanical Systems and Signal Processing*, 28, 212–228.

Mehra, R. K. (1970). "On the Identification of Variances and Adaptive Kalman Filtering." *IEEE Transactions on Automatic Control*, AC-15(2), 175–184.

Myers, K. A., and Tapley, B. D. (1976). "Adaptive Sequential Estimation with Unknown Noise Statistics." *IEEE Transactions on Automatic Control*, 21(4), 520–523.

Nassif, H. H., Gindy, M., and Davis, J. (2005). "Comparison of laser Doppler vibrometer with contact sensors for monitoring bridge deflection and vibration." *Ndt & E International*, Elsevier, 38(3), 213–218.

Pappa, R. S., Elliott, K. B., and Schenk, A. (1993). "Consistent-mode indicator for the eigensystem realization algorithm." *Journal of Guidance, Control, and Dynamics*, 16(5), 852–858.

Park, K.-T., Kim, S.-H., Park, H.-S., and Lee, K.-W. (2005). "The determination of bridge displacement using measured acceleration." *Engineering Structures*, 27(3), 371–378.

Petersen, W., Øiseth, O., Nord, T. S., and Lourens, E. (2018). "Estimation of the full-field dynamic response of a floating bridge using Kalman-type filtering algorithms." *Mechanical Systems and Signal Processing*, Elsevier Ltd, 107, 12–28.

Shumway, R. H., and Stoffer, D. S. (2000). *Time Series Analysis and Its Applications*. Springer-Verlag, New York.

Spencer Jr., B. F., Hoskere, V., and Narazaki, Y. (2019). "Advances in Computer Vision-Based Civil Infrastructure Inspection and Monitoring." *Engineering*.

Tatsis, K., and Lourens, E. (2016). "A comparison of two Kalman-type filters for robust extrapolation of offshore wind turbine support structure response." *Proceedings of the Fifth International Symposium on Life-Cycle Civil Engineering (IALCCE 2016)*, CRC Press, Delft, The Netherlands, 209.